MPI–PhE/94-03
January 1994
H1–02/94-346

Hadronic Calibration of the H1 LAr Calorimeter using Software Weighting Techniques

H.P. Wellisch, J.P. Kubenka, H. Oberlack, P. Schacht

Max–Planck–Institut für Physik
– Werner–Heisenberg–Institut –
80805 Munich (Fed. Rep. Germany)

Contents

1 Introduction **1**

2 Calibration data, methods and optimization procedures **4**

3 Linear calibration for jets **6**

4 Hadronic calibration of the H1–LAr–Calorimeter **13**

4.1 Preselection of electromagnetic showers 13

4.2 Mutual dependence of noise signal and π^0– weighting 21

5 The H1–weighting–module **32**

5.1 Energy parametrization of the weighting parameters 32

5.2 Application of the H1–weighting module for u–quark–jets 38

5.3 Systematic studies on the quality of the hadronic calibration 44

6 Weighting including an estimation of the electromagnetic content of jets **52**

Bibliography **54**

1. Introduction

General remarks

In this note we discuss the weighting part of the hadronic calibration of the H1–LAr–Calorimeter. We use u–quark–jet–data, that had been simulated with Monte–Carlo methods and reconstructed in the default framework of H1 reconstruction software. We will developed a method to calibrate the hadronic response of the liquid argon calorimeter and provide a parametrization of the hadronic calibration as a function of the jet energy.

In the design of the hadronic calibration of the H1–LAr–Calorimeter the following items are of special importance:

- general properties of the jet energy distribution measured on the ideal electromagnetic scale. (This scale gives the correct response for electromagnetic showers. It is called 'ideal', since it is corrected for detector effects like crosstalk or noise cut.)
- method and performance of a cheme for preselecting isolated electromagnetic showers. Isolated electromagnetic showers should not be subject to the hadronic calibration procedure.
- basic properties of the hadronic calibration, such as energy and angular variation of the calibration parameters and achievable energy resolution.
- achievable energy resolution for jets using π^0–weighting–techniques[Dishaw79] [Greiff90][Wellis90] (with and without preselection of electromagnetic showers)
- mutual dependence of noise signal and quality of the hadronic energy measurement using π^0–weighting; optimization of an energy threshold for cells to be considered in the weighting procedure.
- summary description of the procedure employed to calibrate the hadronic response of the H1–LAr–Calorimeter; parametrization of the individual calibration constants as a function of the jet energy.
- description of the algorithm used to apply a given parametrization of the calibration constants in complex event topologies; corresponding systematic studies.
- Check of the quality of the hadronic energy reconstruction for a number of hadronic objects:
    1. u–quark–jet–data from the calibration data

2. u–quark–jet–data on calibration points, but not used in the optimization of the calibration parameters
3. u–quark–jet–data at intermediate jet energies or jet directions far from the calibration points
4. preselected u–quark–jets with high primary electromagnetic content

- investigation of the possibility to further improve the hadronic energy resolution by estimating the electromagnetic content of hadronic showers and including this information in the weighting ansatz directly.

Starting point – energy measurement on the electromagnetic scale

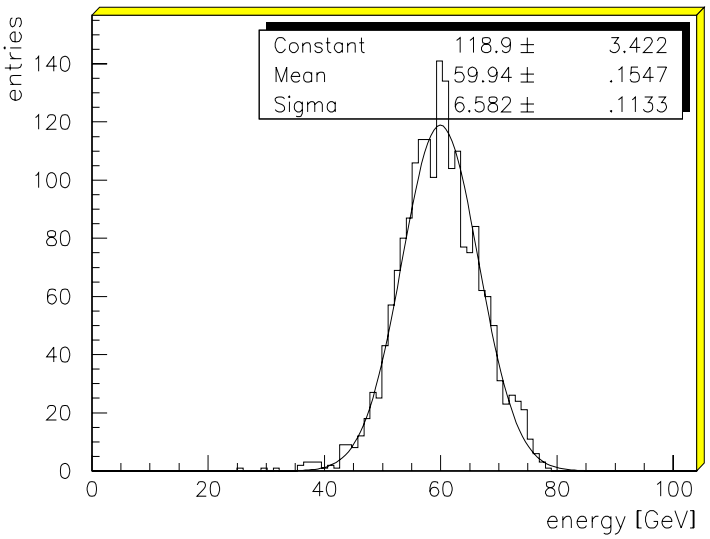

Figure 1.1: *Energy distribution (energy measurement on the electromagnetic scale) for 80 GeV jets in FB2 direction. The full line is a gauß'ian fit to the distribution.*

Figure 1.1 shows the total energy measured in the H1–LAr–Calorimeter on the electromagnetic scale for 80 GeV jets in FB2 direction. The solid line is a gauß'ian fit to the distribution.

In this plot 80 GeV electrons would show up as a sharp peak at 80 GeV. For jets, the distribution is shifted towards lower energies by approximately 30%. (For hadronic energy we aim at an accuracy of the absolute energy measurement of 4%.) The energy resolution is far above the design goal of $50\%/\sqrt{\mathrm{E}}$ to $60\%/\sqrt{\mathrm{E}}$, which would correspond to $\sigma \approx 4$ GeV.

The overall properties of the distribution are similar for all other regions of the calorimeter and all other jet energies. Fitting a gauß'ian function to the data we calculated the most probable energy and the width of the distribution for a couple of jet energies in different calorimeter regions. We show the results together with the width expected for an energy resolution of $55\%/\sqrt{\mathrm{E}}$ in table 1.1. The observed large systematic shifts of

jet direction	energy	$E_0^{mop.,gau\beta}$	$\sigma_{gau\beta}$	$\sigma_{\frac{55\%}{\sqrt{E}}}$
CB3	100 GeV	74.5 GeV	9.08 GeV	4.7 GeV
FB1	80 GeV	60.1 GeV	6.35 GeV	4.3 GeV
	100 GeV	76.2 GeV	7.68 GeV	4.8 GeV
	250 GeV	198.4 GeV	19.17 GeV	7.7 GeV
FB2	80 GeV	59.9 GeV	6.58 GeV	4.3 GeV
	100 GeV	76.3 GeV	8.05 GeV	4.8 GeV
	250 GeV	199.4 GeV	17.79 GeV	7.8 GeV
IFE	40 GeV	27.7 GeV	3.89 GeV	2.9 GeV
	80 GeV	59.0 GeV	7.00 GeV	4.2 GeV
	100 GeV	75.0 GeV	8.16 GeV	4.8 GeV
	250 GeV	194.8 GeV	21.44 GeV	7.7 GeV

Table 1.1: *The most propable energy, found by fitting a gaußian function to the data reconstructed on the ideal electromagnetic scale,* $E_0^{mop.,\mathrm{gau}\beta}$ *and the corresponding energy resolution* $\sigma_{\mathrm{gau}\beta}$ *is shown together with the design energy resolution for a couple of jet energies and directions. At this level, we observe large systematic shifts of the measured energy with respect to the jet energy. The energy resolution is far from the design value.*

the mean measured energy with respect to the jetenergy are due to the well known fact, that for the H1–LAr–Calorimeter the signal ratio of electrons and hadrons of equal energy is not equal to one ($\frac{e}{\pi} \neq 1$). The calorimeter is not compensating. The bad energy resolution is partly due to the hadronic shower fluctuations, partly due to the difference in sampling ratio of the electromagnetic (EMC) and hadronic (HAC) calorimeter part and, especially important for large jet energies, due to the non–compensating behaviour of the LAr–calorimeter.

Apart from the hadronic shower fluctuations, which are an intrinsic property of hadronic cascades, we can significantly reduce the effect of these properties on energy resolution and absolute energy measurement by applying the weighting method.

2. Calibration data, methods and optimization procedures

The data used for the calibration of the hadronic response of the H1–LAr–Calorimeter are u–quark–jets simulated in the H1 detector with Monte Carlo methods in a detailed detektor simulation[Hadr93]. We used GHEISHA 8 over the full range of hadronic shower particle energies in the GEANT 3.14 framework. The electromagnetic component of the jets is simulated with EGS 4 (H1SIM 2.08/00, OTTO 1 1). We simulated jets in five different calorimeter regions (see table 2.1), that correspond to beam directions used in the CERN calibration runs[Hadr93]. The jet energies are 5 GeV, 10 GeV, 20 GeV, 40 GeV, 80 GeV and 100 GeV for all directions and in addition 250 GeV in FB1, FB2 and IF direction. We use 33 calibration points with at least 2000 simulated events at each point. For the purpose of quality studies we simulated jets at intermediate jet energies and directions.

jet direction	polar angle
CB2	79.0°
CB3	53.5°
FB1	34.3°
FB2	25.0°
IF	10.1°

Table 2.1: *Jet directions used in the calibration of the hadronic response of the H1–LAr–calorimeter.*

The calibration methods used in the following are the linear calibration and the weighting technique (π^0–weighting)[Dishaw79][Greiff90][Wellis90].

For linear calibration the following relation holds between the cell energy measured on the ideal electromagnetic scale[1] (E^0_{cell}) and the final reconstructed energy ($E_{cell}(E^0_{cell})$):

$$\left\{ E_{cell}(E^0_{cell}) \;=\; C \cdot E^0_{cell} \right\}_{EMC/HAC}$$

For the weighting method we have:

$$\left\{ \frac{E_{cell}(E^0_{cell})}{E^0_{cell}} \;=\; C_1 \cdot exp(-C_2 \cdot E^0_{cell}/V_{cell}) \;+\; C_3 \right\}_{EMC/HAC}$$

[1] In the following this will always mean after perfect dead material corrections for crack effects

V_{cell} is the geometrical volume of a calorimeter cell.

The parameters C_i are optimized for EMC (electromagnetic calorimeter part) and HAC (hadronic calorimeter part) separately in two minimal χ^2– fits minimizing the difference of the energy reconstructed, $E_{reco.}$, and the energy deposited, $E_{depo.}$, in EMC and HAC respectively, applying the boundary condition, that the mean energy reconstructed in EMC or HAC equals the mean energy deposited in EMC or HAC respectively.

$$\left\{ \chi^2 \;=\; \sum_{events} \left(E_{reco.} \;-\; E_{depo.}\right)^2 \Big|_{\langle E_{reco.}\rangle \;=\; \langle E_{depo.}\rangle} \right\}_{EMC/HAC}$$

Using the deposited energies we take effects of dead material in front of the calorimeter and leakage effects into account automatically. This is possible only when calibrating on MC data.

Several methods to calculate $E_{reco.}$ have been investigated. We use the general ansatz:

$$\left\{ E_{reco.} \;=\; \sum_{cells} E_{cell}(E^0_{cell}) + E_{select.} \right\}_{EMC/HAC}$$

The various methods differ in the restrictions posed on the calorimeter cells for which the hadronic calibration will be applied and in the treatment of the remaining energy, $E_{select.}$.

- When using calibration without additional conditions the above sum runs over all cells of the corresponding calorimeter part, and thus

$$E_{select.} \;=\; 0.$$

- For calibration with preselection of electromagnetic showers we apply a preselection of electron and gamma candidate energy clusters (cluster = local conglomeration of calorimeter cells[Wellis91]). The selected clusters will not be included in the hadronic calibration procedure, but treated separately. Apart from a correction factor, f_{noise}, necessary to correct for the influence of the noise cut, the energy of preselected clusters is measured on the ideal electromagnetic scale.

$$E_{select.} \;=\; \sum_{select.} E^0_{cell} \cdot f_{noise}$$

- For calibration with an energy threshold on cells subject to the weighting procedure the above sum of reconstructed energies runs over all cells above a certain energy threshold. Cells below this threshold are kept on the electromagnetic scale. This may avoid the enhancement of noise energy due to π^0–weighting. For $E_{select.}$ we obtain in this case:

$$E_{select.} \;=\; \sum_{E<E_{thresh.}} E^0_{cell}$$

3. Linear calibration for jets

Using the available monte carlo data (u–quark–jets) we studied the energy and angular dependence of a hadronic calibration and the achievable energy resolution for the simple case of linear calibration:

$$\left\{ E_{cell}(E^0_{cell}) \;=\; C \cdot E^0_{cell} \right\}_{EMC/HAC}$$

A topological $2/4{\cdot}\sigma_{noise}$ noise cut was applied. In this kind of noise suppression all calorimeter cells with energy above $4{\cdot}\sigma_{noise}$ are selected. In addition direkt neighbours of these cells with energies larger than $2{\cdot}\sigma_{noise}$ are kept. The parameter C was found in the optimization procedure described in chapter 2. The resulting values of C are plotted as a function of the jet energy in fig. 3.1 and 3.2 for the electromagnetic and for the hadronic calorimeter part.

The general properties of the energy dependence of the calibration parameters are similar for all jet directions and both calorimeter parts. The calibration parameters drop rather fast with increasing jet energy and show an approximately asymptotic behaviour at high energies. Fitting an exponential function with a small additional linear term to the data we obtained a reasonably good energy parametrization of the calibration constants for all polar angles. The bandwidth of the variation of the calibration parameter is different in EMC and HAC. In EMC the calibration constant covers the range from 1.1 to 2.0, in HAC it covers the range from 1.3 to 2.0. The difference in bandwidth can be understood from the difference of about a factor of two in the signal to noise ratios in EMC and HAC. The different asymptotic values of the calibration parameters in EMC and HAC can be explained by the difference in the e/π–ratio in EMC and HAC and the finite primary electromagnetic content of the jets, that is deposited predominately in the electromagnetic calorimeter, rendering the calibration constant in EMC closer to unity than in the hadronic calorimeter part.

The angular variation of the calibration is shown in the figures 3.3 and 3.4 for EMC and HAC respectively. The bandwidth of the angular variation is similar in EMC and HAC. It ammounts to 10% in each calorimeter part. In EMC the calibration constant increases rapidly from IF to FB1 for practically all jet energies. In the CB region we find a plateaulike behaviour.

In HAC we find the strongest variations in the forward region, IF to FB1, too. Indications of a plateau in the CB area are visible, but the angular dependence of the calibration parameters in this region is much stronger than that observed in the electromagnetic calorimeter part.

Figure 3.5 shows the energy resolution achieved with this method. The dotted line is a fit to the data using the parametrization of the energy resolution (equation 3.1) of [Fabian89] for jet energies larger than 5 GeV:

$$\frac{\sigma}{E} = \sqrt{\frac{A^2_{samp.}}{E} + B^2_{const.} + \frac{C^2_{noise}}{E^2}} \tag{3.1}$$

The noise term C_{noise} has been omitted. The contributions of the individual terms to the energy resolution are shown in table 3. The solid line in figure 3.5 shows the goal of $\frac{55\%}{\sqrt{E}}$.

jet direction	$A_{samp.}$	$B_{const.}$
CB2	$(65.5 \pm 0.9)\%$	$(3.41 \pm 0.30)\%$
CB3	$(65.9 \pm 0.9)\%$	$(3.77 \pm 0.29)\%$
FB1	$(68.1 \pm 0.7)\%$	$(3.87 \pm 0.12)\%$
FB2	$(71.3 \pm 0.7)\%$	$(4.08 \pm 0.11)\%$
IF	$(69.4 \pm 0.7)\%$	$(3.33 \pm 0.12)\%$

Table 3.1: *Statistical and constant contribution to the energy resolution as found by fitting the energy parametrization of the energy resolution to the data.*

In the investigated energy regime, already with this primitive ansatz, the energy resolution is better than 100 $\%/\sqrt{E_0}$ and thus substantially improved in comparison to the results obtained for the measurement on the ideal electromagnetic scale. For the precision we aim for, however, the resolution is not sufficiently good, especially not at high jet energies. Linear calibration should not be used without a preceding weighting step.

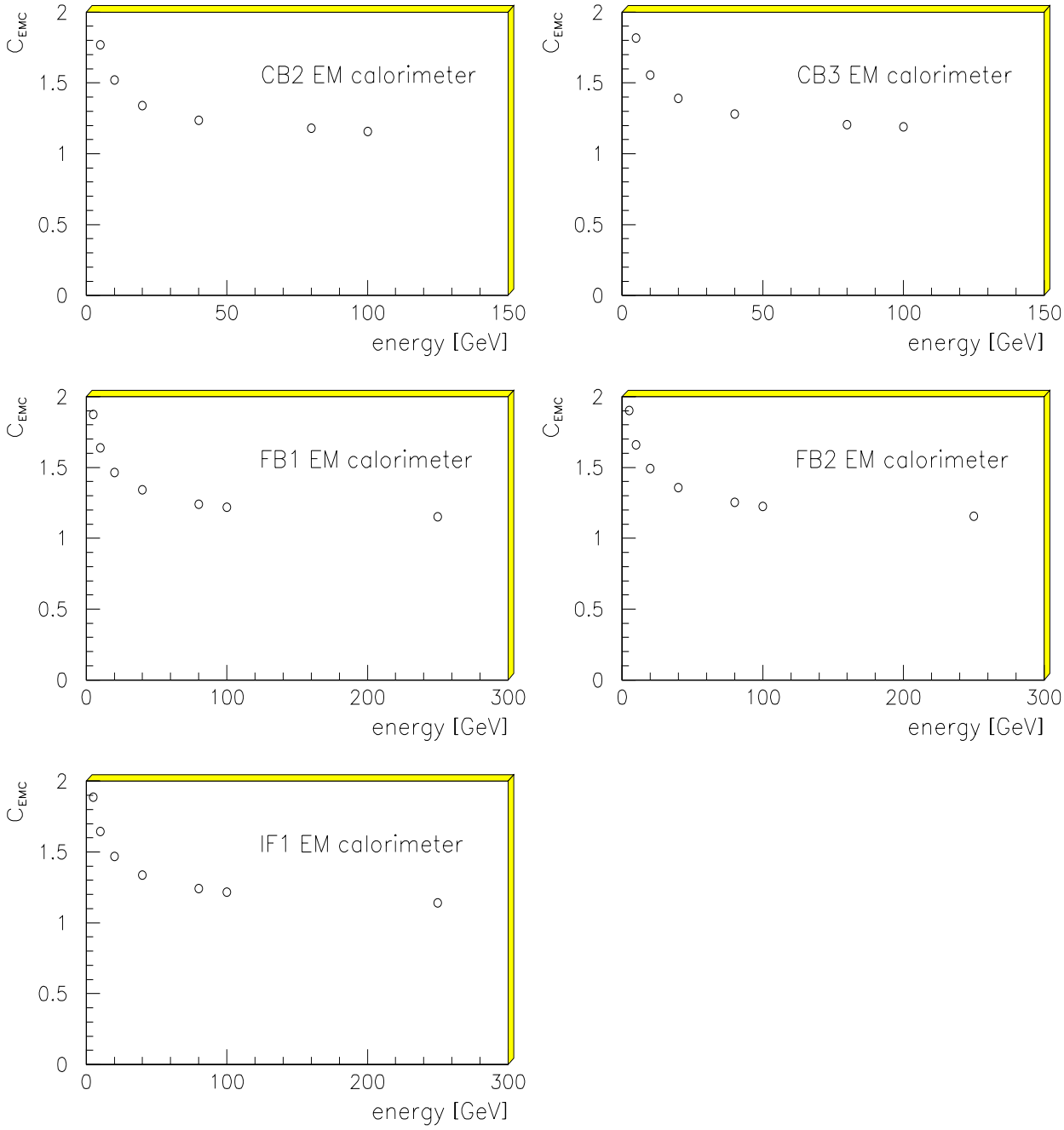

Figure 3.1: *Calibration parameters (linear calibration) in the electromagnetic calorimeter part for the various jet directions as a function of the jet energy.*

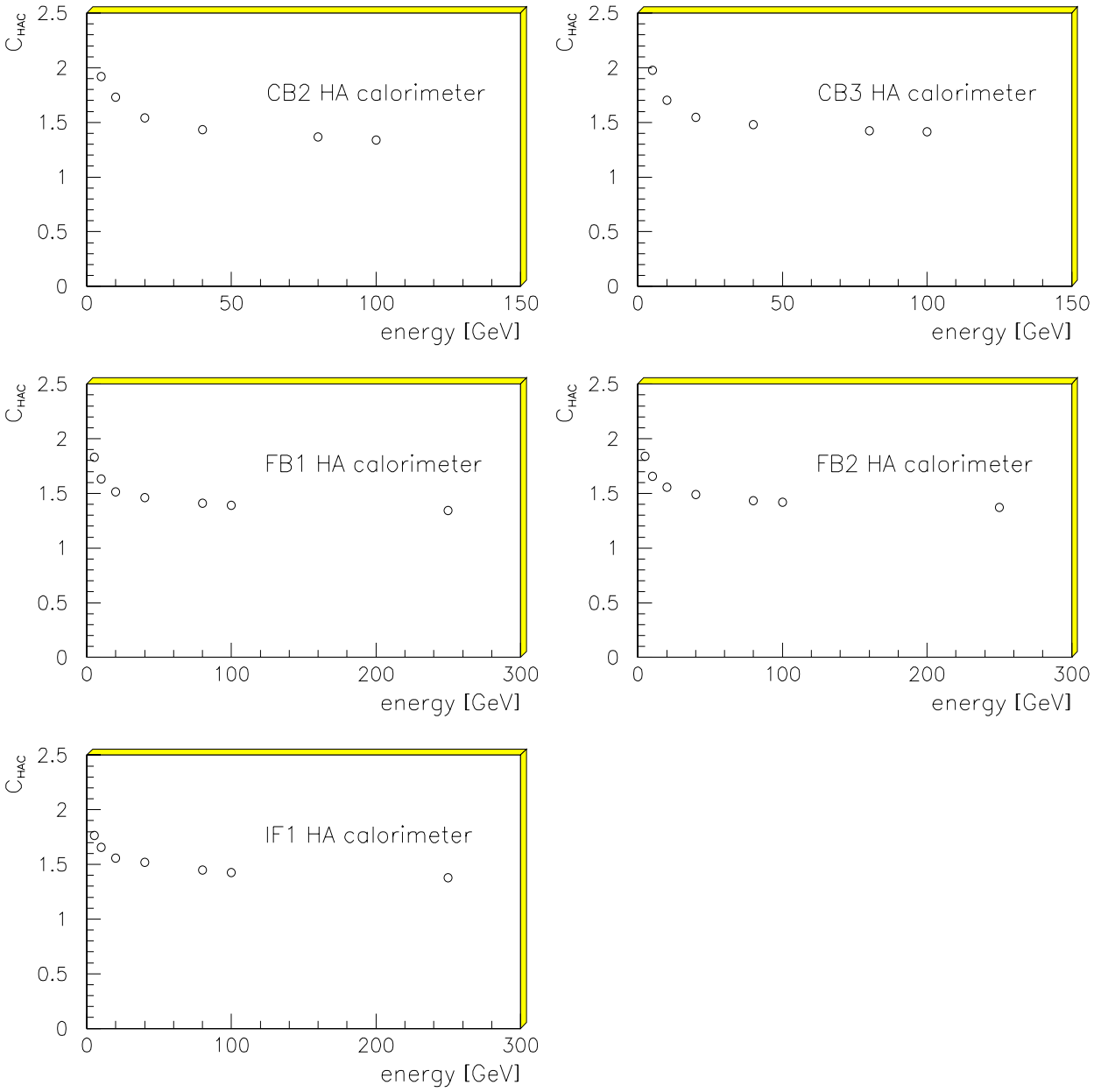

Figure 3.2: *Calibration parameters (linear calibration) in the hadronic calorimeter part for the various jet directions as a function of the jet energy.*

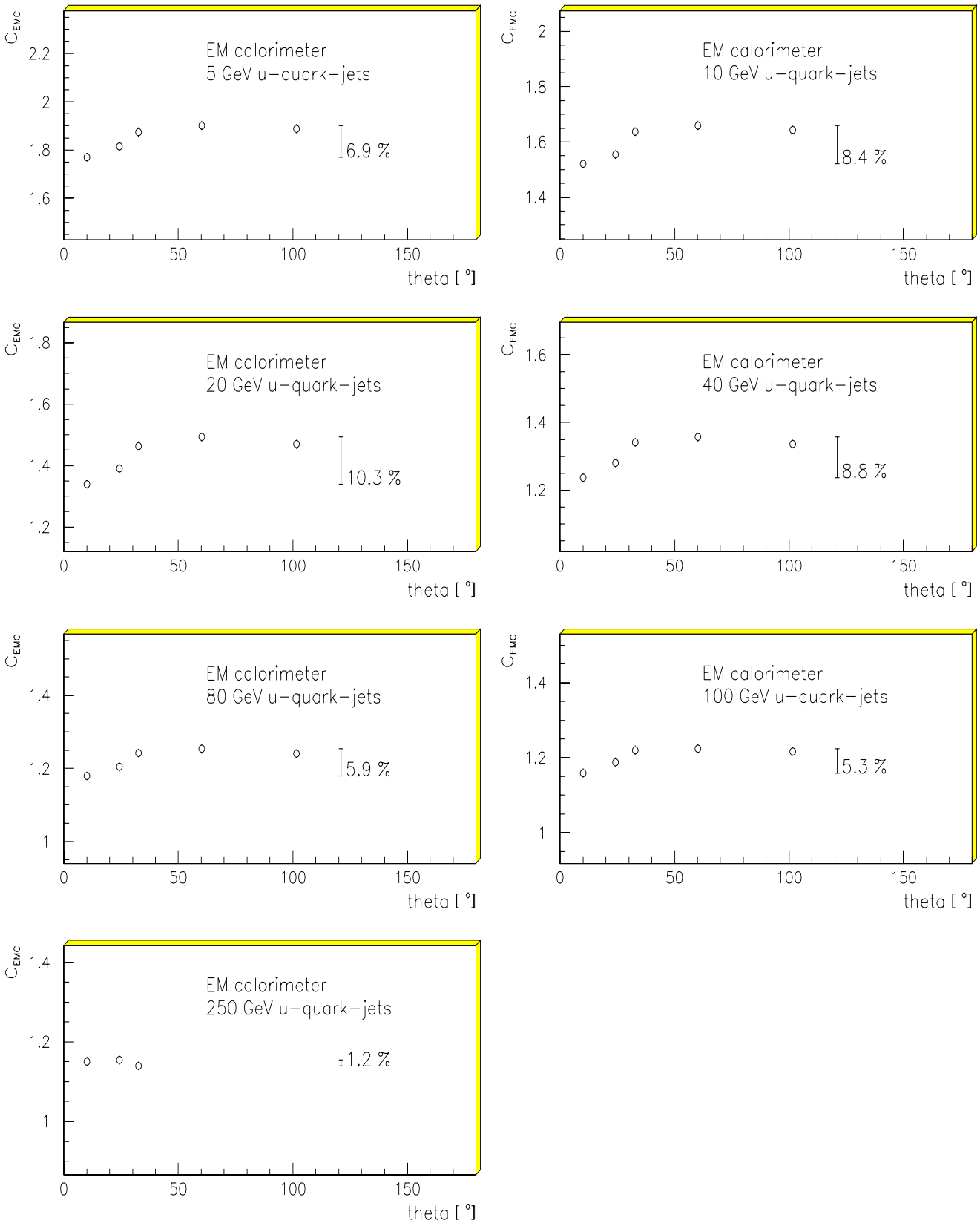

Figure 3.3: *Calibration parameters (linear calibration) in the electromagnetic calorimeter part for various jet energies as a function of jet direction.*

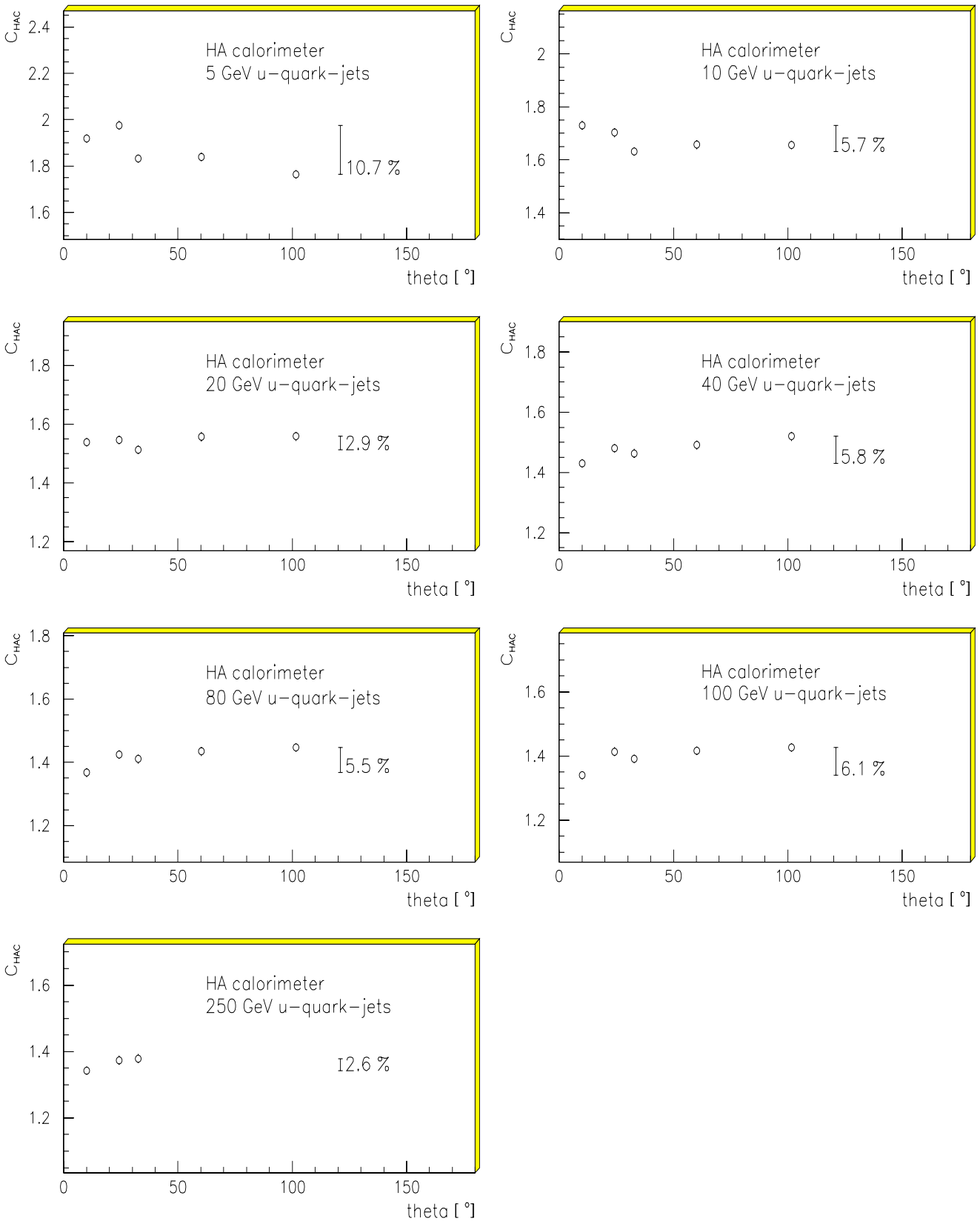

Figure 3.4: *Calibration parameters (linear calibration) in the hadronic calorimeter part as a function of jet direction for various jet energies.*

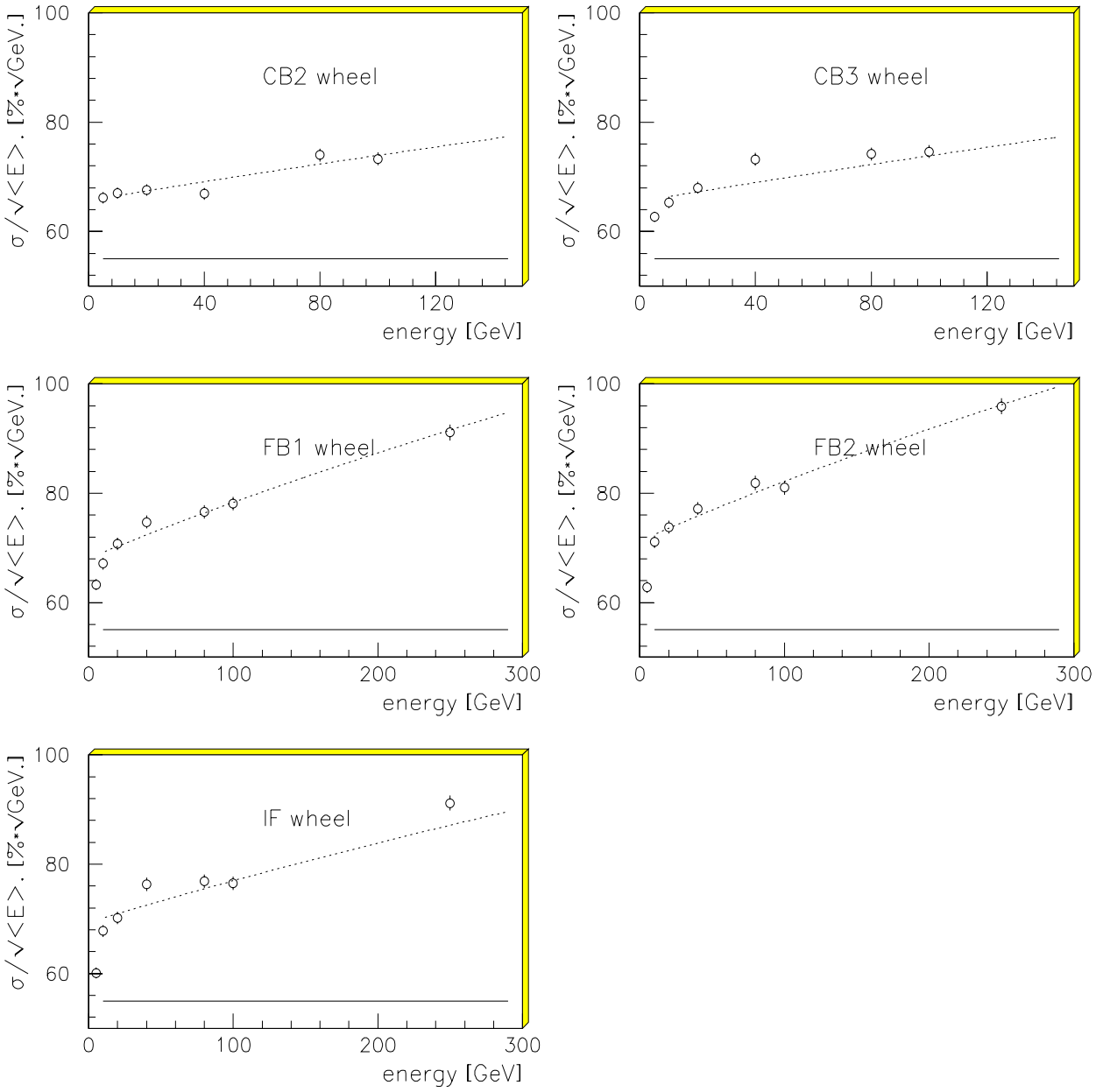

Figure 3.5: *Energy resolution achieved in the various calorimeter regions as a function of the jet energy, using linear calibration. The dashed curve is a parametrization of the energy resolution for jet energies larger than 5 GeV, the full line is the goal resolution.*

4. Hadronic calibration of the H1–LAr–Calorimeter

In order to obtain a hadronic calibration of the H1–LAr–Calorimeter matching the design goal on energy resolution and absolute energy measurement, we applied the π^0–weighting method introduced by J.P. Dishaw [Dishaw79] and first employed by the CDHS collaboration and developed it further. As a weighting function we used an exponential ansatz similar to that described in [Greiff90],

$$\left\{ \frac{E_{cell}(Q_{cell})}{Q_{cell}} \;=\; C_1 \cdot exp(-C_2 \cdot Q_{cell}) \;+\; C_3 \right\}_{EMC/HAC}$$

making the following conceptional changes:

- The deposited charge, Q_{cell}, was replaced by the energy measured on the ideal electromagnetic scale. This gives us the possibility to calibrate the calorimeter response with Monte Carlo data.
- In the exponent the energy density was used in stead of the deposited charge. This way the energy [Wellis90] and presumably also the angular dependence of the calibration is strongly reduced.
- A preselection of electromagnetic showers is performed. Preselected showers stay unweighted and, apart from a small correction for effects of the noise cut, they are kept on the ideal electromagnetic scale.
- Cell energies below a threshold of $3 \cdot \sigma_{noise}$ stay unweighted. This way the influence of the hadronic calibration on the total noise signal is minimized.
- In contrast to all preceding studies the weighting parameters were optimized independently for the electromagnetic and the hadronic calorimeter part in two subsequent optimization procedures. This removes unwanted correlations of the calibration constants in EMC and HAC.

4.1 Preselection of electromagnetic showers

To improve the local precision of the energy reconstruction, a preselection of electromagnetic clusters is performed. The response of the H1–LAr–Calorimeter to electromagnetic showers is calibrated correctly on the ideal electromagnetic scale. Thus

it is useful not to apply the hadronic calibration for clearly isolated electromagnetic showers, and to take this into account in the optimization of the weighting parameters.

The basis of the preselection procedure is the H1–LAr–Clustering [Wellis91]. It provides the possibility to disentangle electromagnetic and hadronic showers, to some extent even in crowded event topologies with high local energy densities.

The preselection procedure

One method to identify electromagnetic showers is to utilize simple algorithms developed for particle identification. These so-called estimators have been designed and optimized by Y.Sirois et al. They transform a given efficiency ϵ for electron identification to a window of values for the selected estimator. The individual estimators have been parametrized as a function of position and energy of a cluster. The parametrizations have been tuned on CERN–calibration–data [Sirois93].

In the hadronic calibration of the LAr–Calorimeter the following estimators have been used:

- EAK0: Ratio of the energy of a cluster reconstructed in the first longitudinal layer of the calorimeter to the total energy of the cluster.
- EAH4: Ratio of the energy in the four neighbouring cells of maximal charge density of a cluster to the total energy of the cluster.

In order to find a method, that allows to identify a maximal fraction of all electromagnetic showers, that are separated in space from hadronic showers, and to minimize simultaneously the misidentification probability for hadronic energy for jets in the energy range from 5 GeV to 250 GeV all over the entire calorimeter, we systematically studied the effect of the estimators for various values of ϵ in various estimator combinations. For each individual test, the following quantities have been investigated:

$< f_{tag} >$ – Mean ratio of the electromagnetic component of the preselected clusters (in MC available) to the total energy deposited in EMC by electromagnetic showers. (All secondary electromagnetic components of hadronic showers in the EMC are included.)

$< f_{fake} >$ – Mean ratio of the hadronic component of all preselected clusters (in MC available) to the total energy of the generated hadrons.

$N_{t,85\%}$ – Number of jets for which more than 85% of the total energy deposited by electromagnetic showers in EMC was identified correctly.

$N_{f,15\%}$ – Number of jets for which more than 15% of the energy of all generated hadrons was faked.

When applying the estimaters individually, the quality of the preselection of electromagnetic showers is satisfactory for all reasonably high values of ϵ ($\epsilon > 85\%$), but wheel dependent. The faked hadronic energy amounts to up to 15%, which is to large for our purposes. Since the preselected energy will be kept on the electromagnetic scale, in

these scenarios a significant fraction of the hadronic energy would stay uncalibrated, resulting in a local systematic error in the absolute energy measurement of 10% to 50% (table 1.1). Results are presented in table 4.1 exemplary for EAK0, $\epsilon = 95\%$.

The assignment of hadronic energy can be significantly improved by using AND–combinations of the estimaters, sacrificing the amount of preselected electromagnetic energy to some extent. The method described in the following is one possible compromise between effective preselection of electromagnetic energy and good assignment of hadronic energy:

- Only clusters with energies larger than 1 GeV are considered in the preselection.
- More than 80 % of the cluster energy is inside the electromagnetic calorimeter part.
- Clusters whose energy center of gravity is closer to a ϕ–crack than 44 mrad are not considered in the preselection.
- The clusters fulfil both the criteria EAK0 and EAH4 at 99% electron identification efficiency.

The results obtained in this scheme are shown in figure 4.1 and 4.2. The amount of misidentified hadronic energy is about 1.5% on average. It is always below 4%. It will be shown, that this is sufficiently small, that no significant degradation of the jet energy resolution is observable.

The mean preselection efficiency for electromagnetic energy is 20% to 40% for all jet energies and directions. The smaller efficiencies for 5 GeV jets are due to the cluster energy cutoff of 1 GeV. The drop at very high energies is due to the fact, that the decrease of the jet opening angle with increasing jet energy leads to a stronger spatial overlap of electromagnetic and hadronic components of a jet, what makes it a priori impossible to separate them.

Typical distributions of f_{tag} and f_{fake} are shown in fig. 4.3. The f_{tag}–distribution shows one peak at $f_{tag} = 1$ and one peak at $f_{tag} = 0$. The peak at $f_{tag} = 0$ contains those events, for which electromagnetic and hadronic parts of the jet overlap to a large extent. They cannot be separated. The peak at $f_{tag} = 1$ shows, that with the given method it is possible for a certain fraction of the jets to identify the total energy, that was deposited in the EMC by electromagnetic showers. The f_{fake}–distribution shows a peak at $f_{fake} = 0$ and a tail towards larger misidentified hadronic energy fractions.

The peak structure described above is observed for practically all jet energies and directions. Independent of the jet energy for 10% to 20% of the jets more than 85% of the total electromagnetic component of the showers can be isolated.

The method described above is used in the hadronic calibration of the H1–LAr–Calorimeter to preselect electromagnetic showers.

jet energy	jet direction	$< f_{tag} >$	$< f_{fake} >$	N_{total}	$N_{t,85\%}$	$N_{f,15\%}$
5 GeV	CB2	56.86 %	6.45 %	2000	641	317
	CB3	58.81 %	7.75 %	2000	653	375
	FB1	60.78 %	8.55 %	2000	651	446
	FB2	62.08 %	9.44 %	2000	648	490
	IFE	58.38 %	9.01 %	2000	595	483
10 GeV	CB2	56.46 %	7.18 %	1999	625	349
	CB3	63.48 %	8.58 %	1999	708	435
	FB1	63.46 %	8.50 %	1999	652	426
	FB2	69.21 %	10.93 %	1999	773	601
	IFE	55.76 %	0.09 %	1999	463	452
20 GeV	CB2	56.04 %	7.07 %	1998	632	350
	CB3	64.69 %	9.18 %	1936	768	495
	FB1	65.52 %	8.67 %	1899	724	426
	FB2	75.22 %	11.73 %	1843	882	641
	IFE	54.97 %	8.33 %	1998	492	413
40 GeV	CB2	60.73 %	6.53 %	1995	856	282
	CB3	73.46 %	10.42 %	1998	1179	637
	FB1	70.52 %	9.51 %	1996	1004	537
	FB2	80.54 %	12.55 %	1999	1231	809
	IFE	58.64 %	8.87 %	1997	669	501
80 GeV	CB2	71.71 %	5.79 %	1972	1260	164
	CB3	83.50 %	9.94 %	2000	1561	559
	FB1	79.06 %	10.17 %	2000	1407	616
	FB2	87.32 %	13.13 %	1940	1551	887
	IFE	67.66 %	9.32 %	2000	1004	552
100 GeV	CB2	76.66 %	5.41 %	1969	1397	100
	CB3	85.68 %	9.27 %	1995	1628	446
	FB1	80.43 %	9.66 %	2000	1500	550
	FB2	89.39 %	13.16 %	2000	1680	924
	IFE	71.19 %	9.33 %	1954	1129	522
250 GeV	FB1	89.61 %	8.36 %	1193	1059	147
	FB2	95.43 %	10.78 %	1040	993	230
	IFE	87.92 %	8.28 %	1251	1060	165

Table 4.1: *Summary on the preselection of isolated electromagnetic showers using one estimator only for the example of the EAK0 estimator for an electron identification efficiency of 95%. We show for the available jet data the mean fraction of the electromagnetic content of the jets in EMC, that has been identified ($< f_{tag} >$), the mean fraction of the energy of the generated hadrons, that was misinterpreted ($< f_{fake} >$), the number of events used for the study (N_{total}), the number of events, for which more than 85% of the electromagnetic content deposited in EMC has been correctly identified ($N_{t,85\%}$), and the number of events for which more than 15% of the primary hadronic content of the jet has been faked ($N_{f,15\%}$). It is common to all one–estimator–approaches, that $< f_{tag} >$ is high, but also $< f_{fake} >$ is up to 15%, which is too large for the purpose of hadronic calibration.*

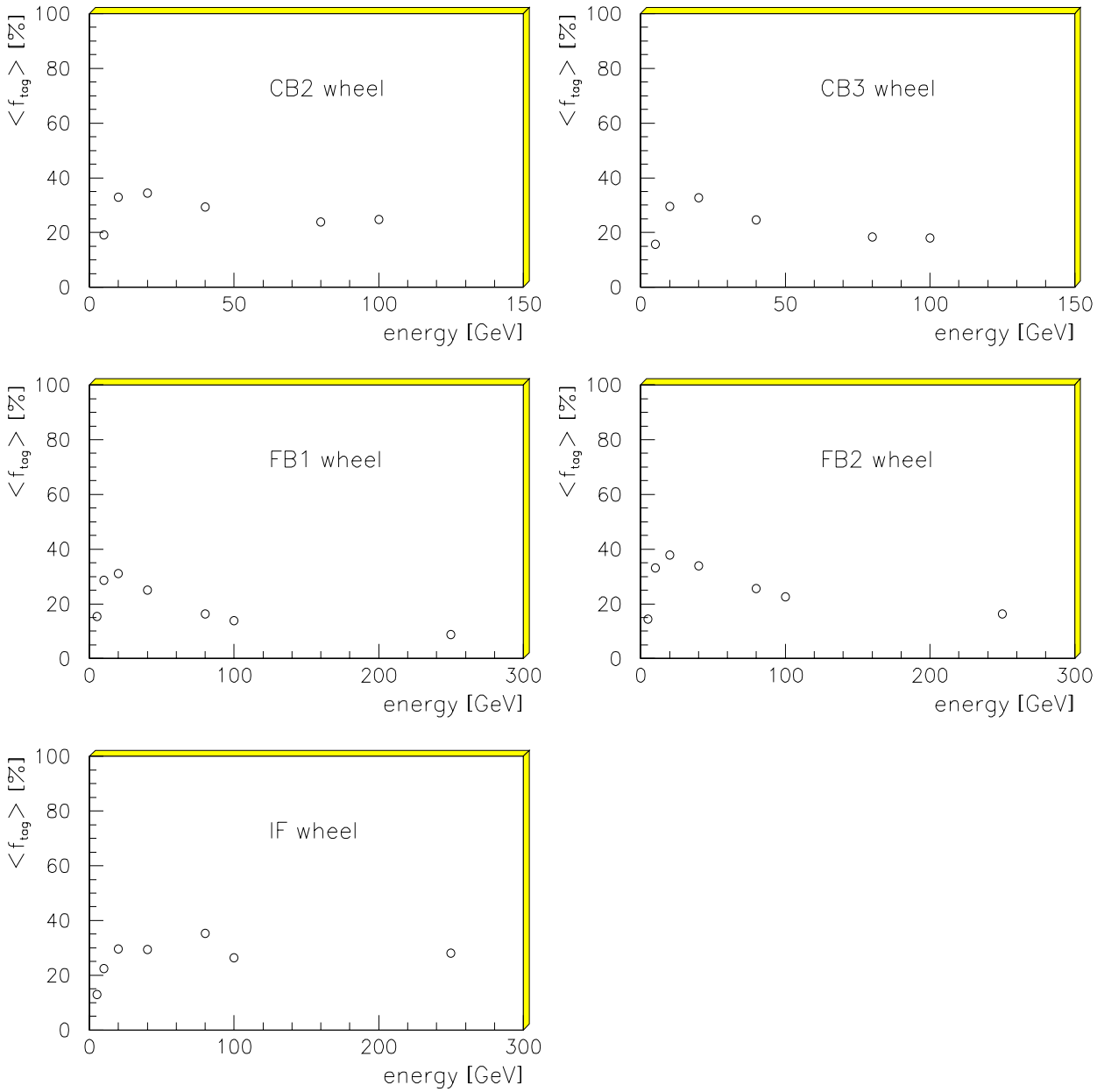

Figure 4.1: *Mean efficiency of the preselection of electromagnetic showers for the various calorimeter regions as a function of jet energy, using the given preselection method. The low values at 5 GeV jet energy are due to a 1 GeV cluster energy cutoff in the preselection. The decrease towards high energy is due to the decrease of the jet opening angle.*

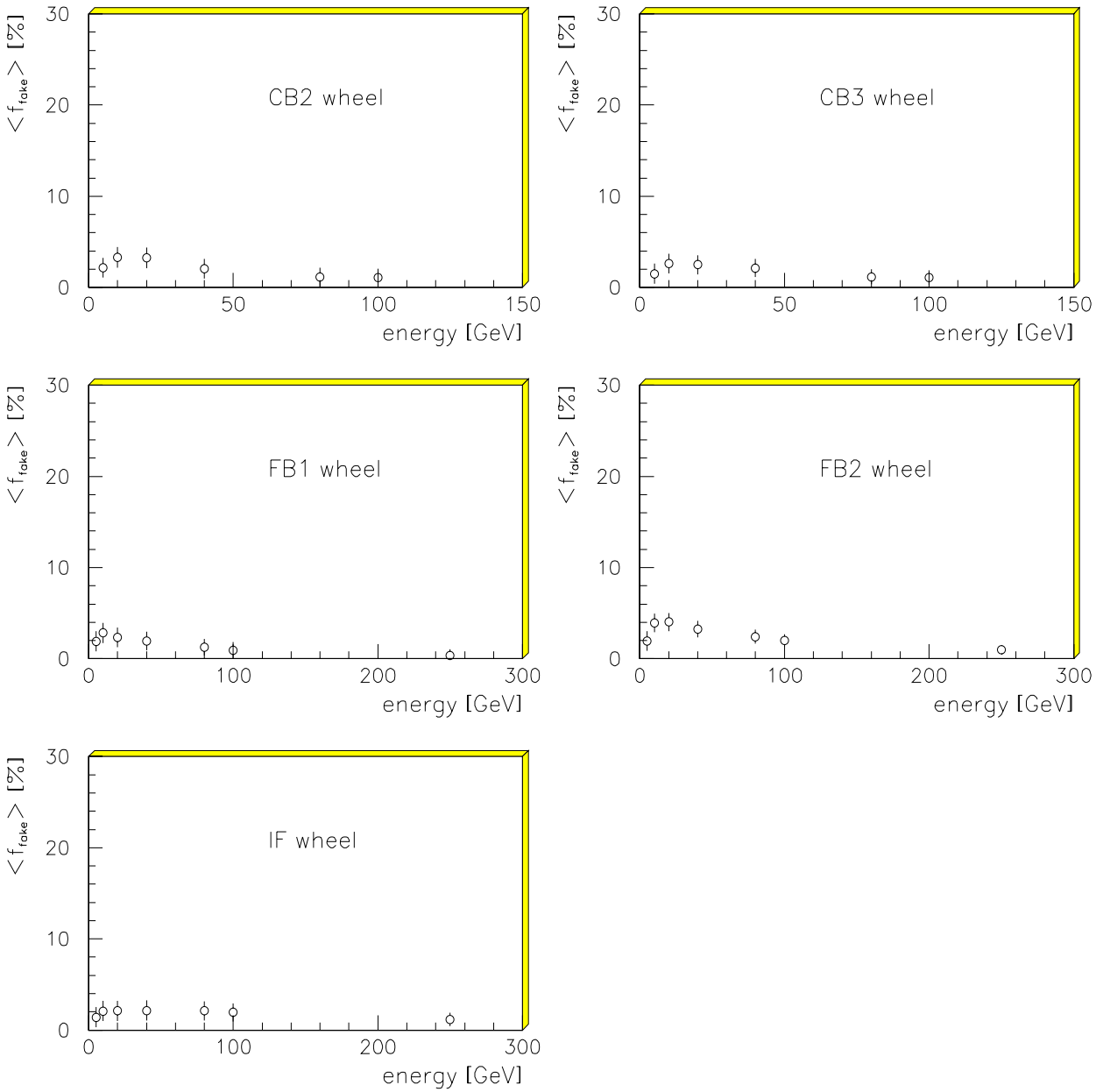

Figure 4.2: *Mean fraction of misidentified hadronic energy in the various calorimeter regions as a function of jet energy using the given preselection method. It will be shown, that this misidentification rate is small enough, that no deterioration of the hadronic energy resolution is observed.*

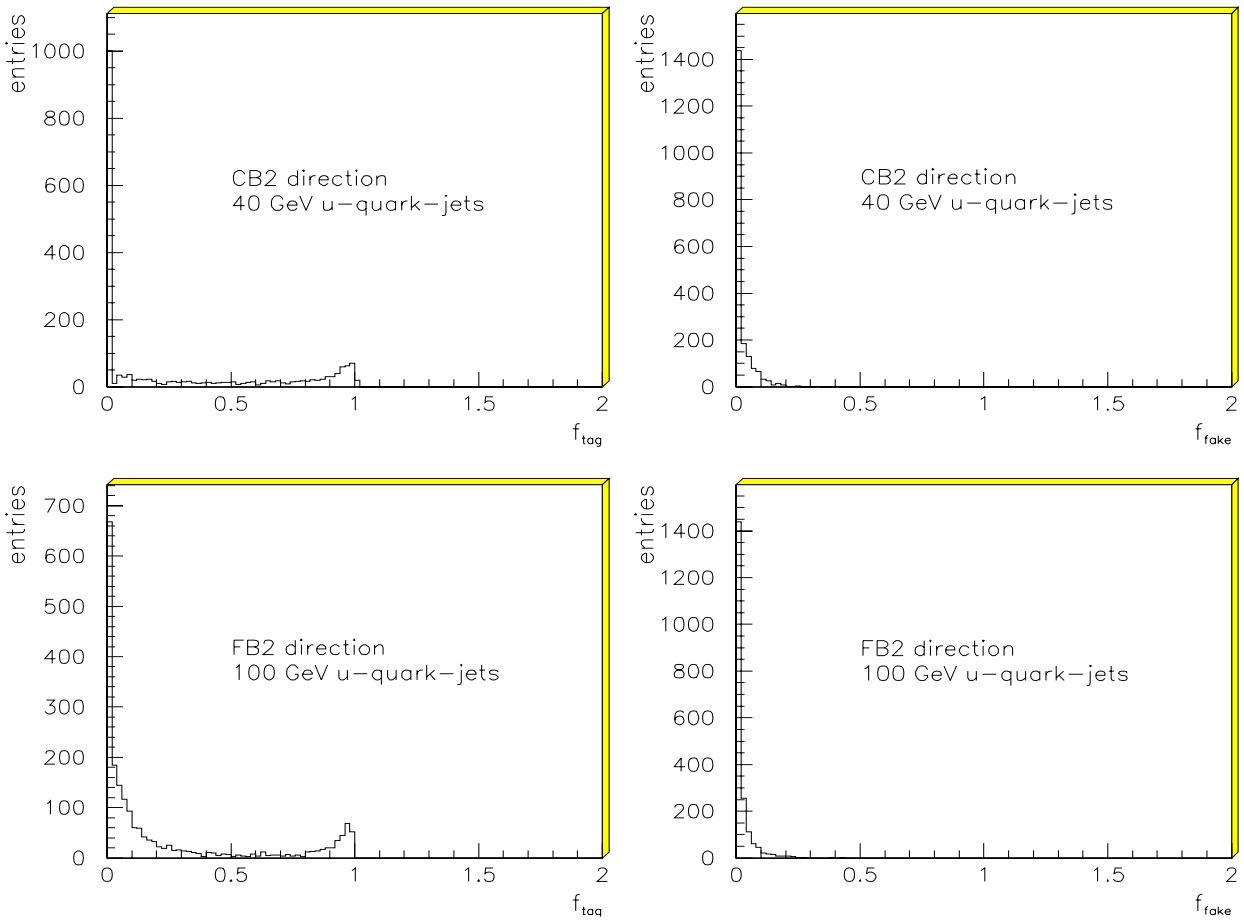

Figure 4.3: *Distribution of the efficiency of the preselection of electromagnetic showers, f_{tag}, and the fraction of hadronic energy wrongly classified as electromagnetic, f_{fake}, for the example of 40 GeV jets in CB2 direction and 100 GeV jets in FB2 direction for the preselection procedure used in calibrating the hadronic response of the H1–LAr–Calorimeter.*

Noise cut correction for electromagnetic clusters

In order to reconstruct energy in isolated electromagnetic showers, we start at the ideal electromagnetic scale.

To further improve the calibration for electrons for a particular noise cut, we estimated the influence of the noise cut on the electron calibration for a number of cuts. For this purpose we simulated electrons at 20 GeV energy in the electromagnetic section of the calorimeter, 200 events per wheel. The starting points of the electrons were choosen at the front faces of the individual stacks [Kube94]. The simulated electromagnetic showers were reconstructed using perfect corrections for energy losses in dead material (Monte Carlo quantity) and the ideal electromagnetic scale (a.e.: [Gayler91]). From a comparison of the reconstructed energy and the energy deposited in the calorimeter (Monte Carlo quantity) we obtained the correction factors given in table 4.2. For the investigated noise cuts the change of the electron calibration due to the noise cut is always smaller than 6%. The statistical precision of the results is about 0.2%.

calorimeter part	noise cut						
	no cut	$1{\cdot}\sigma_{noise}$	$2{\cdot}\sigma_{noise}$	$3{\cdot}\sigma_{noise}$	$2/4{\cdot}\sigma_{noise}$	$4{\cdot}\sigma_{noise}$	$5{\cdot}\sigma_{noise}$
CB1E	1.011	1.027	1.033	1.041	1.033	1.046	1.054
CB2E	1.011	1.024	1.037	1.039	1.032	1.046	1.050
CB3E	1.006	1.024	1.040	1.046	1.042	1.054	1.059
FB1E	0.999	1.010	1.023	1.034	1.025	1.046	1.049
FB2E	1.001	1.013	1.028	1.040	1.030	1.049	1.057
IFE	1.003	1.014	1.030	1.042	1.032	1.050	1.058

Table 4.2: *Ratio of the energy deposited to the energy reconstructed on the electromagnetic scale for 20 GeV electrons in the electromagnetic calorimeter parts for various noise cuts.*

The energy dependence of these corrections was tested in the CB2 part of the calorimeter for a $2/4{\cdot}\sigma_{noise}$ cut. Decreasing the electron energy from 20 GeV to 5 GeV results in an absolute increase of the corrections by 1%. In the following the corrections found for 20 GeV electrons are applied for all preselected clusters independent of the cluster energy.

Influence of the preselection of electromagnetic showers on the hadronic energy resolution

In fig.4.4 we show as a function of the jet energy the energy resolution achieved with linear calibration in the various directions of the calorimeter with (full points) and without (open circles) preselection of electromagnetic showers. The topological $2/4{\cdot}\sigma_{noise}$ noise cut was used. The corresponding corrections of the electromagnetic scale were applied for preselected clusters.

The energy resolutions achieved with the two methods are identical within errors for most data points. An improvement of the jet energy resolution by applying the pre-

selection of electromagnetic showers is visible for jet energies smaller than 20 GeV or greater than 80 GeV.

4.2 Mutual dependence of noise signal and π^0– weighting

Influence of the noise cut on the quality of hadronic calibration

In order to study the influence of the noise cut on the hadronic energy resolution we optimized weighting parameters for various noise cuts. Starting without noise cut, we rose the cut in steps of $1{\cdot}\sigma_{noise}$ from $0{\cdot}\sigma_{noise}$ to $5{\cdot}\sigma_{noise}$. In addition we used the topological $2/4{\cdot}\sigma_{noise}$ cut. The study has been performed in two jet directions (CB2, FB1) for two jet energies each (5 GeV, 80 GeV). Since the weighting procedure starts from the electromagnetic scale, the reference point of the study is the noise cut dependence of the energy reconstruction on the electromagnetic scale.

Fig. 4.5 shows the influence of the noise cut on the energy reconstruction on the ideal electromagnetic scale. For a jet energy of 5 GeV we find a steady decrease of the measured energy with increasing noise cut (up to 50%). At the same time the energy resolution, σ/E is degraded from about 25% to about 40%. For higher jet energies the influence of the noise cut is weaker, but still significant. For 80 GeV jets both the measured energy and the energy resolution vary by 10% to 15% in the range of noise cuts investigated. This behaviour is to be expected for any kind of hadronic calibration, that starts from the electromagnetic scale. Deviations from this behaviour are special features of the individual hadronic calibration method.

Fig. 4.6 shows the influence of the noise cut on the energy resolution in the case of weighting (full points). Here, using the preselection of electromagnetic showers and the proper correction of the electromagnetic scale, for each individual noise cut the weighting parameters were fitted in the optimization procedure described in chapter 2. The resolutions are normalized to those obtained for a $2/4{\cdot}\sigma_{noise}$ topological noise cut.

If the relative improvement of the energy resolution via weighting is independent of the noise cut, we expect the energy resolution to behave as it has been found for the electromagnetic scale. The open circles in fig. 4.6 show this behaviour.

We find for large jet energies, that after weighting the change of the energy resolution as a function of the noise cut agrees within errors with that expected from the measurement on the ideal electromagnetic scale. There are no peculiarities of the weighting method.

For jets with an energy of 5 GeV we find agreement with the expected behaviour without any special relation of noise cut and weighting for noise cuts above $1{\cdot}\sigma_{noise}$. For the weakest noise cuts we find better energy resolutions than expected.

The energy resolution achievable depends strongly on the signal to noise ratio. Starting from $5{\cdot}\sigma_{noise}$, with decreasing noise cut (which is aequivalent to increasing signal to noise ratio) we find a strong improvement of the energy resolution even for high jet energies (up to 15% for 80 GeV jets). For small jet energies this tendency is additionally enhanced when using the weighting method (improvements by up to 45%).

Noise cut dependence of the weighting parameters

The dependence of the form of the weighting function on the noise cut is of essential interest. Unless the weighting parameters are retuned for a changed noise cut, we a priori expect for the weighting method a strong dependence of the absolute energy calibration and the energy resolution on the noise cut. The reason is the exponential energy density dependence of the weighting function. In order to systematically investigate the size of this noise cut dependence, we studied the changes of the absolute energy calibration and the resolution when applying the calibration optimized for an $2/4{\cdot}\sigma_{noise}$ noise cut for other noise cuts.

In fig. 4.7 we show for the CB2 and FB1 directions for jet energies of 5 GeV and 80 GeV the resolution and the mean relative difference between deposited and reconstructed energy as a function of the noise cut (open circles). In addition, we show the variation of the energy measured on the ideal electromagnetic scale (stars) and the energy resolution obtained when optimizing the weighting parameters for each noise cut individually (full points). Each data point is normalized to the value found for the $2/4{\cdot}\sigma_{noise}$ cut. In this plot the flexibility of the weighting method can be seen especially impressively. The energy resolution is slightly degraded when applying the calibration tuned for an $2/4{\cdot}\sigma_{noise}$ noise cut at other cut values. For most of the noise cuts, especially for cuts above $1{\cdot}\sigma_{noise}$, the absolute energy measurement is practically unaffected. Apart from the variation of the energy measured on the electromagnetic scale we find only marginal contributions due to the dependence of the form of the weighting function on the noise cut.

It is important, that the energy resolutions obtained when applying the parameters optimized for a $2/4{\cdot}\sigma_{noise}$ noise cut in most cases agrees [1] within errors with the resolution obtained when optimizing the weighting parameters for each noise cut individually. This means in practice, that in case of changes of the signal to noise ratio, for example due to a rescaling of the electromagnetic scale, it is not necessary to retune the weighting parameters in a time consuming procedure, but it is sufficient to rescale the weighted energy, or the parameters C_1 and C_3 in the weighting ansatz, by an appropriate factor.

Enhancement of the noise signal in the weighting procedure

Since the e/π–ratio is not equal to one in the H1–LAr–Calorimeter, and the weighting function depends exponentially on the energy density, the application of weighting im-

[1] except for unrealistically low noise cuts

plies an enhancement of the contribution of noise to the total measured energy. In the following this enhancement of the noise signal in the weighting procedure will be investigated. We use random triggers from the H1–cosmic–runs, spring 1992, run#10632, 1000 events.

We found the expected strong dependence of the total noise energy on the noise cut (Fig. 4.8). On the electromagnetic scale the mean total noise energy amounts to about 55 GeV for a $2{\cdot}\sigma_{noise}$ noise cut. With increasing noise cut it decreases continuously down to 0.55 GeV for a $5{\cdot}\sigma_{noise}$ noise cut. The topological $2/4{\cdot}\sigma_{noise}$cut is a noise treatment, that is optimized with respect to noise suppression and the reconstruction efficiency for low energy particles. The mean integral noise energy in random triggers is 2 GeV for this cut.

For the lowest available jet energy we determined weighting parameters for two different noise treatments; the $2/4{\cdot}\sigma_{noise}$ cut and without noise cut. The preselection of electromagnetic showers and the proper correction of the electromagnetic scale for clusters associated with electromagnetic showers were used. The calibration found for the low energy jets was then applied to random events. Hot and extremely noisy channels were removed from the analysis.

We show in fig.4.9 for both sets of weighting parameters the weighting induced enhancement of the total noise signal as a function of the noise cut.

We found, that the enhancement of noise in the weighting procedure depends on both, the noise cut applied in the optimization of the weighting parameters and the noise cut applied in the energy reconstruction. For the two different sets of weighting parameters we found a difference in the enhancement of the noise signal of 40% to 50%. This is consistent with the effect expected due to the noise cut dependence of the energy measured for low energy jets on the electromagnetic scale for the two noise cuts. This is the the expected, 'trivial' part of the noise cut dependence. As a function of the noise cut applied on the data in the energy reconstruction the enhancement of noise decreases with increasing noise cut. For a overall $2/4{\cdot}\sigma_{noise}$cut the mean noise energy is enhanced by a factor of 2.17. It is 4.3 GeV in total. For very small values of (x,Q^2) this energy is of the same size as the total energy deposited by the particles of the hadronic final state in the barrel and backward part of the LAr calorimeter.

In the following we will present a method that allowes to minimize the enhancement of the total noise signal due to weighting.

Weighting above an energy threshold

In order to minimize the enhancement of the noise signal in the hadronic calibration, and thus to minimize the contribution of noise to the total measured energy, we keep all cells with energies below a certain energy threshold ($n \cdot \sigma_{noise}$) on the electromagnetic scale, and apply weighting only for cells with higher energies.

The energy threshold will be optimized with respect to achievable energy resolution and enhancement of noise energy for the case of a $2/4{\cdot}\sigma_{noise}$ topological noise cut. For

this purpose we investigate the energy resolution in CB2 and IF direction at 5 GeV, 20 GeV and 100 GeV jet energy for various threshold values (Fig. 4.10).

In general we find a slow degradation of the energy resolution with increasing threshold. This degradation is especially strong for low jet energies. For thresholds above $4{\cdot}\sigma_{noise}$ we see sizable effects for most jet energies and directions. Thresholds up to $3{\cdot}\sigma_{noise}$ leave the energy resolution practically untouched.

In the following we investigate the effect of an energy threshold on cells to be weighted on the enhancement of the total noise signal. For this purpose we optimized weighting parameters for 5 GeV jets for the $2/4{\cdot}\sigma_{noise}$ cut at each individual energy threshold. We applied this low energy hadronic calibration for the random events described above and NC events ($Q^2 \in [30GeV^2, 100GeV^2]$; $x \in [10^{-2}, 3 \cdot 10^{-2}]$) simulated with monte carlo methods overlayed event by event with noise from the random triggers. We included only those cells which contain noise signal only (in MC available) in our investigations. Hot and extremely noisy channels were removed from the analysis. In fig. 4.11 the enhancement of noise as a function of the energy threshold for weighting is shown for both event samples.

We found a reduction of the enhancement of noise with increasing energy threshold. A plateau in the range from $3{\cdot}\sigma_{noise}$ to $4{\cdot}\sigma_{noise}$ is visible. The difference between random triggers and physic events as well as the observed plateau are due to the topology dependence of the $2/4{\cdot}\sigma_{noise}$ noise cut. They are due to the fact, that cells with energies between $2{\cdot}\sigma_{noise}$ and $4{\cdot}\sigma_{noise}$ are accepted only, if a directly neighbouring cell shows a signal above $4{\cdot}\sigma_{noise}$. In this procedure the number of noise cells kept in the interval $E_{cell} \in [2{\cdot}\sigma_{noise}, 4{\cdot}\sigma_{noise}]$ is considerably larger in physic events than in random triggers for obvious reasons. The number of noise cells additionally skipped by increasing the threshold decreases rapidly when the threshold approaches $4{\cdot}\sigma_{noise}$. Since the weighting parameters had been retuned for each individual threshold to fix the absolute energy measurement for low energy jets, the enhancement of the noise signal rises close to $4{\cdot}\sigma_{noise}$.

In the following for the calibration of the H1–LAr–Calorimeter the $2/4{\cdot}\sigma_{noise}$ noise cut in combination with a $3{\cdot}\sigma_{noise}$ energy threshold for weighting is used. The noise cut and the energy threshold both are essential parameters of the calibration. The calibration parameters and systematic errors given in the following, are applicable and reproduceable only using identical conditions.

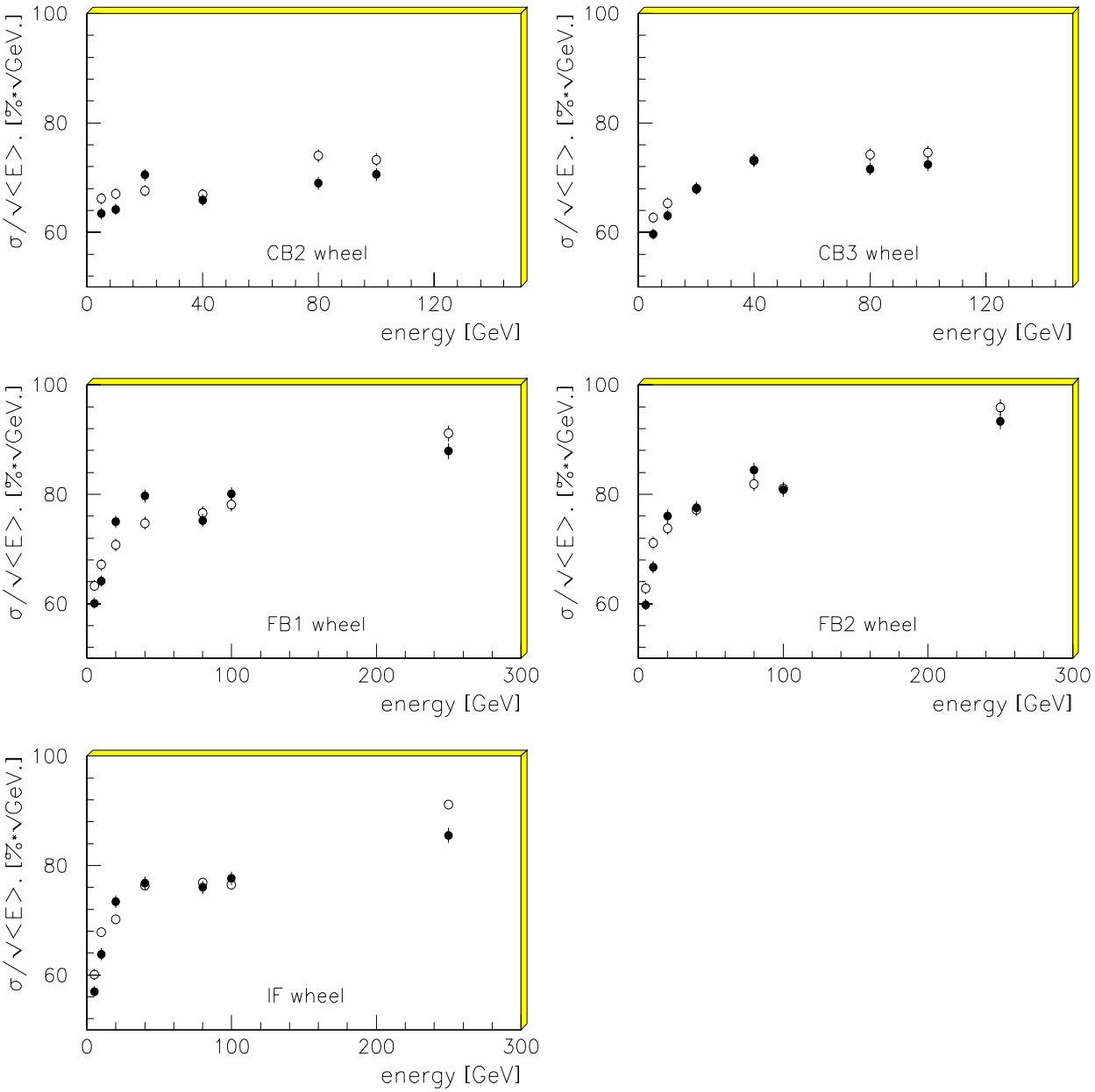

Figure 4.4: *Energy resolution obtained in the various calorimeter regions using linear calibration, shown as a function of the jet energy (full points). In addition we show the energy resolution obtained when applying the given preselection method (open circles).*

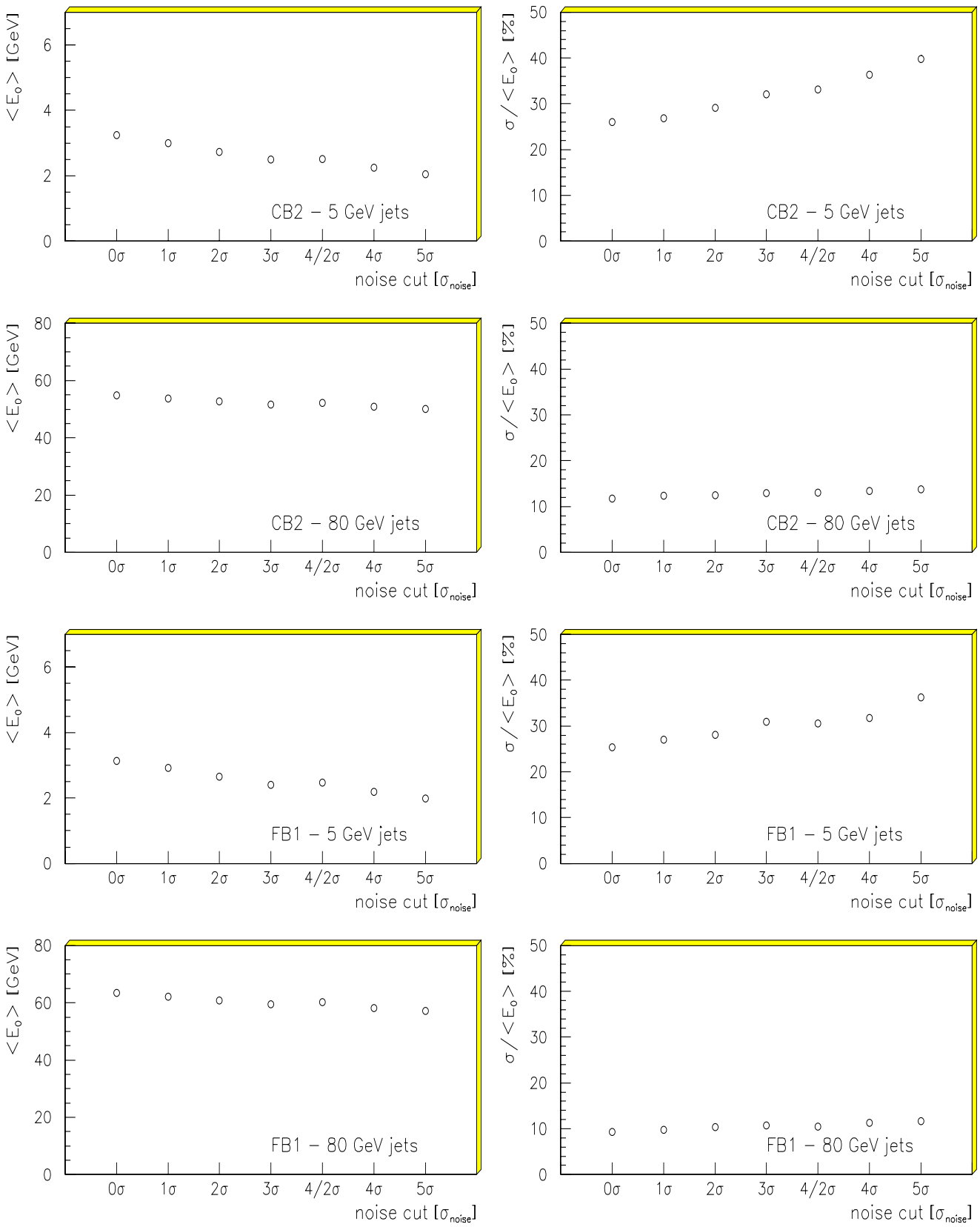

Figure 4.5: *Typical energy resolution and mean reconstructed energy as found on the electromagnetic scale for selected jet directions and energies as a function of the noise cut.*

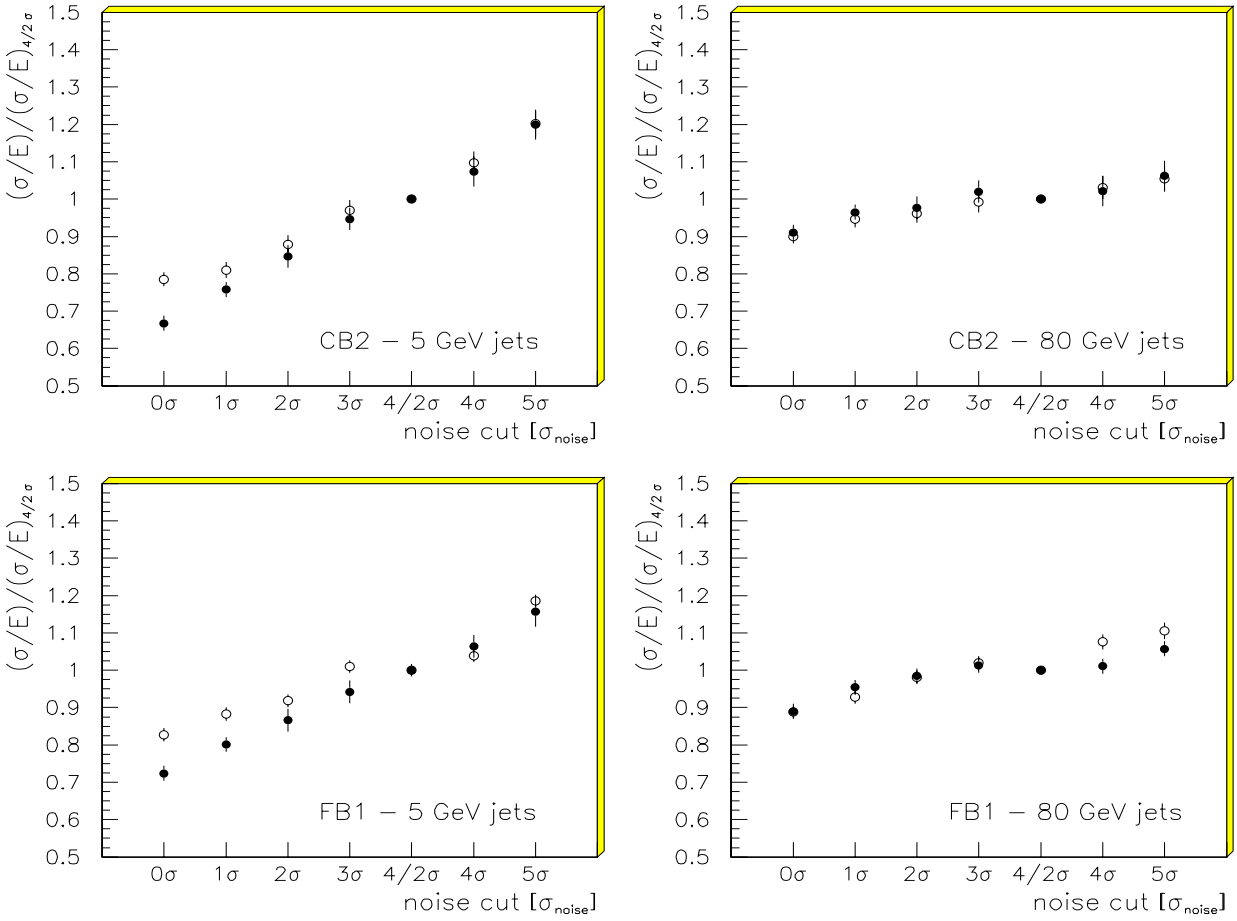

Figure 4.6: *Energy resolution normalized to the resolution found for a 2/4 ·σ_{noise} noise cut as a function of the noise cut applied in the optimization of the calibration parameters. The open circles show the behaviour expected from the noise cut dependence of the energy measurement on the electromagnetic scale.*

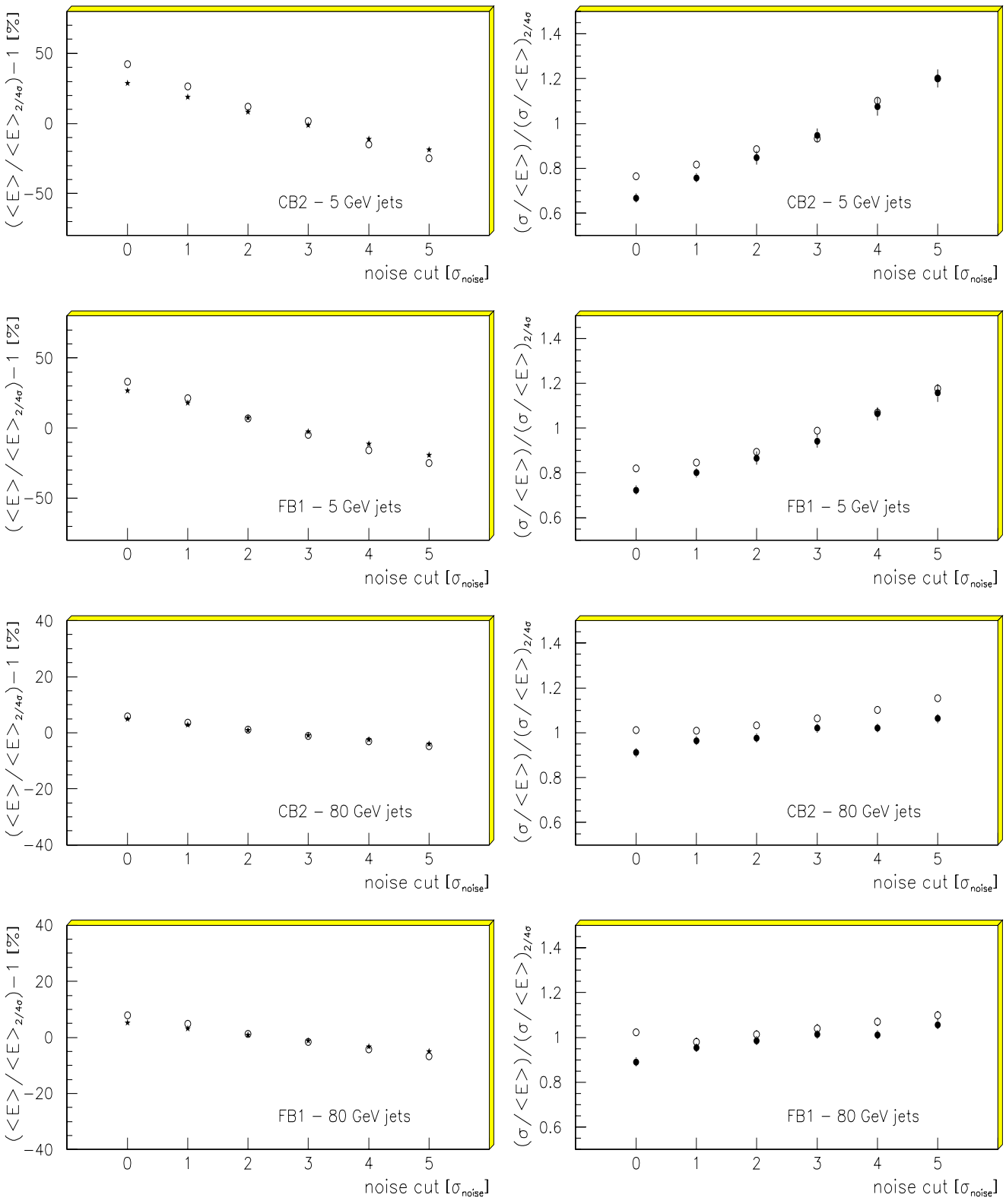

Figure 4.7: *Energy resolution and mean reconstructed energy as a function of the noise cut. As reference point we used the values found for a 2/4 ·σ_{noise} noise cut. The open circles show the results obtained when applying the weighting parameters optimized for a 2/4 ·σ_{noise} cut. The stars show the behaviour of the energy measured on the electromagnetic scale, the full points show the results found when optimizing weighting parameters for each noise cut individually.*

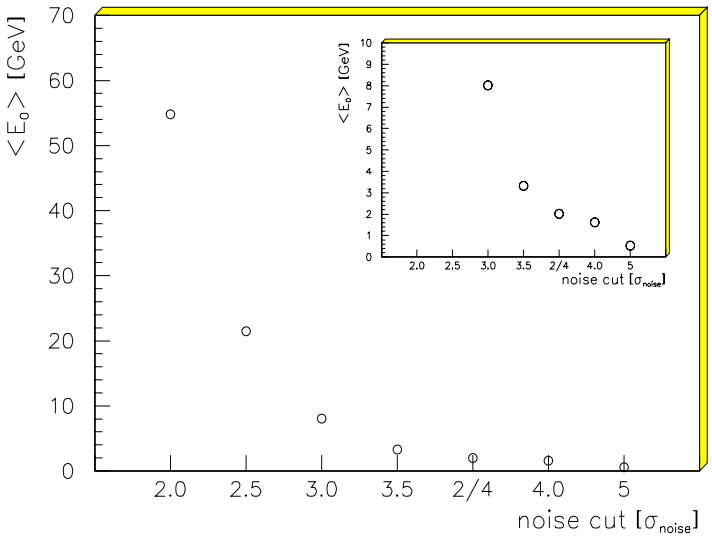

Figure 4.8: *Noise signal on the electromagnetic scale summed over the entire LAr–calorimeter as a function of the noise cut.*

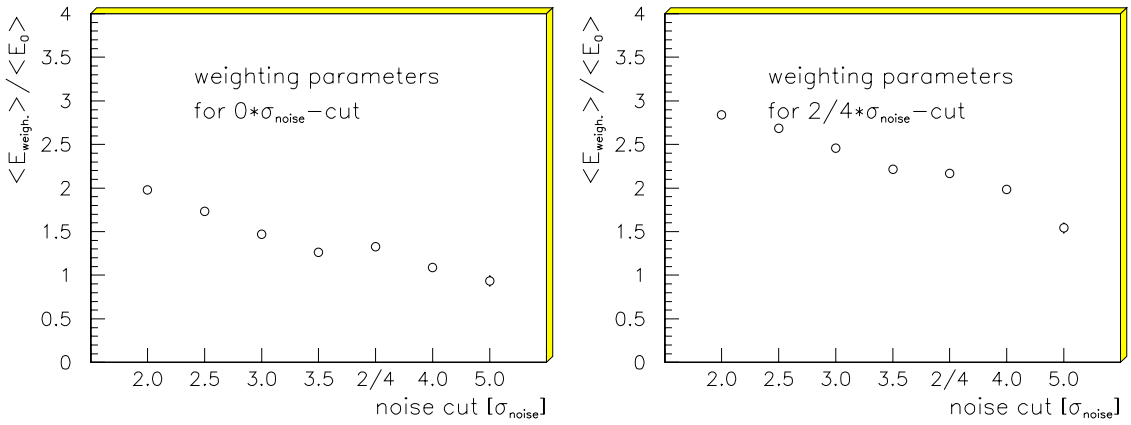

Figure 4.9: *Enhancement of the noise signal in the weighting procedure as a function of the noise cut for random triggers from H1 cosmic runs and for NC events.*

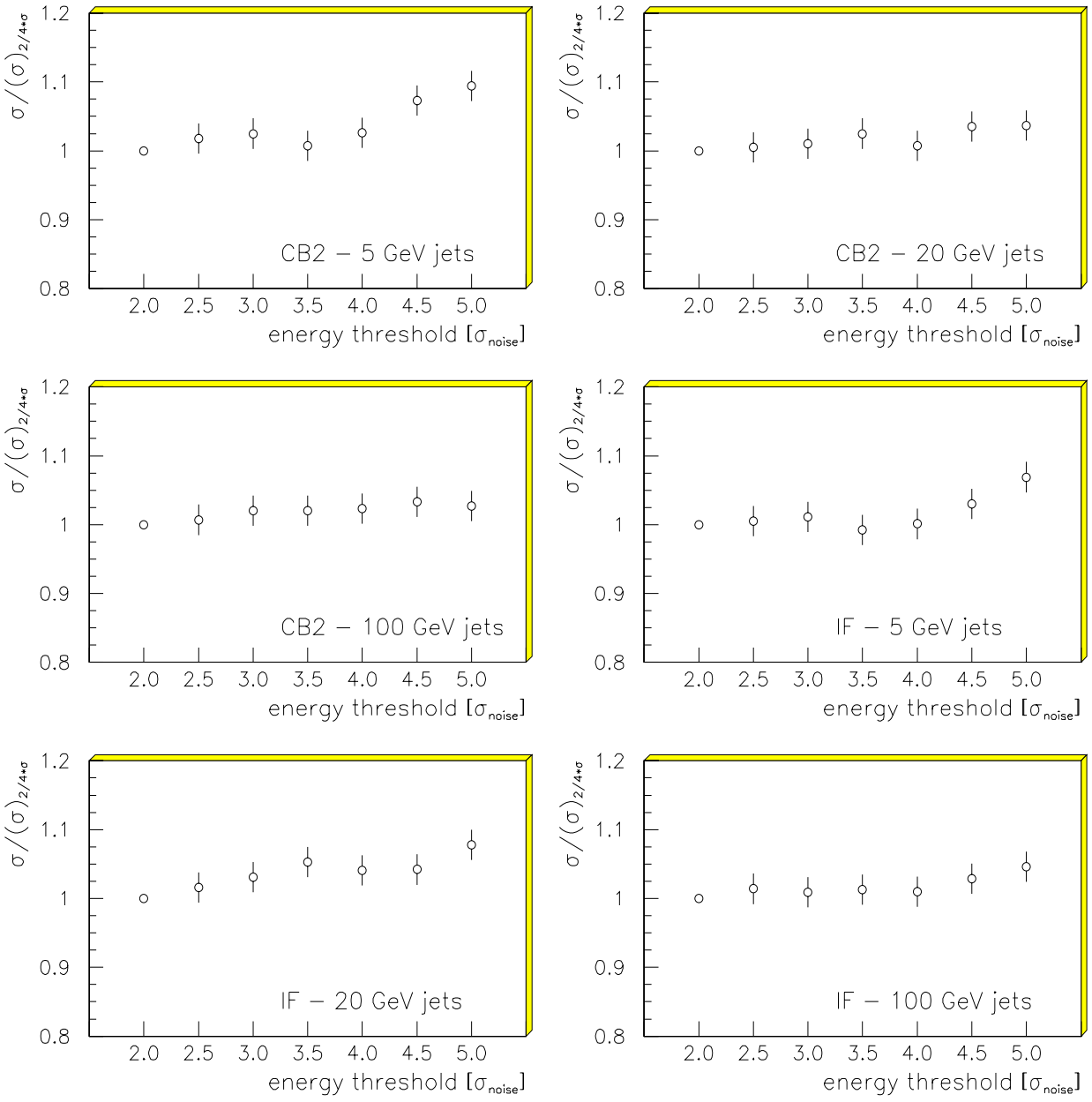

Figure 4.10: *Energy resolution achieved as a function of the energy threshold. Weighting was applied only for cells with energies above the threshold.*

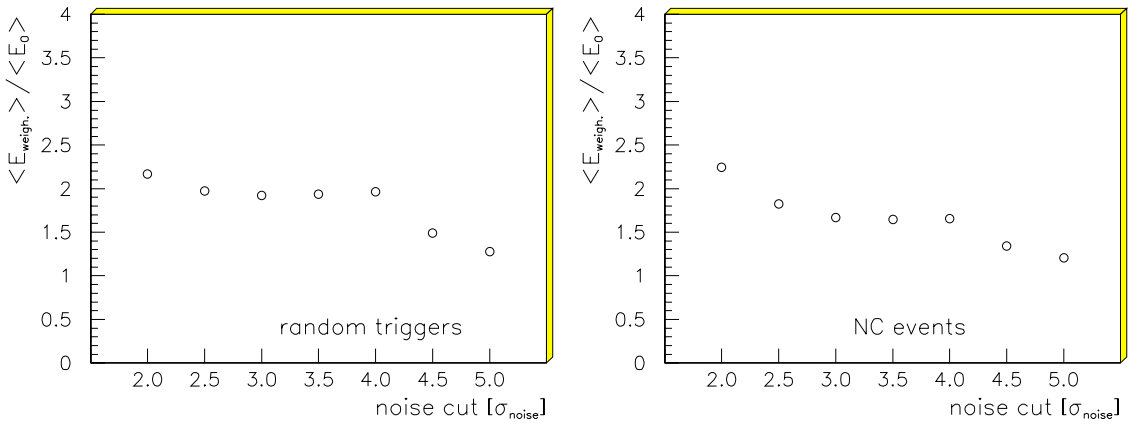

Figure 4.11: *Enhancement of the noise energy as a function of the energy threshold for weighting. After a 2/4 $\cdot\sigma_{noise}$ noise cut the weighting parameters applied for random and NC events were optimized for each threshold value individually. Only cells above the threshold were considered in the weighting procedure. Cells below the threshold were kept on the electromagnetic scale.*

5. The H1–weighting–module

In this chapter we will summarize the basic concepts of the weighting part of the hadronic calibration of the H1–LAr–Calorimeter and show results on the performance of this module.

The weighting part of the hadronic calibration of the H1–LAr–Calorimeter is based on the following principles:

- Hadronic calibration starts at the ideal electromagnetic scale (after dead material correction).
- A $2/4 \cdot \sigma_{noise}$ topological noise cut is used.
- Ideal electromagnetic scale for cells below $3 \cdot \sigma_{noise}$.
- Preselection of electromagnetic showers.
- Correction for the influence of the noise cut on electromagnetic showers.
- An exponential weighting function using energy density in the exponent[Wellis90].
- Parametrization of the weighting parameters as function of energy, interpolation in θ.
- Application of the parametrization for complex event topologies in a conelike algorithm.

The aim of this work was to achieve for jets an absolute precision of the energy measurement better than 4% and an energy resolution in the order of $50\%/\sqrt{E}$ to $60\%/\sqrt{E}$. Moreover, and more ambitious, the quality of the absolute energy measurement should be independent of the composition of the jets in terms of electromagnetic and hadronic showers.

5.1 Energy parametrization of the weighting parameters

In fig. 5.1 we show the energy resolutions achieved when optimizing weighting parameters for each individual set of jet energy and direction. These values give the absolute limit on the resolution achievable with the given method. The dotted line is the parametrization of the energy resolution achieved with the linear calibration ansatz, the full line indicates the goal of $55\%\sqrt{E}$.

$$\left\{ \frac{E_{cell}(E^0_{cell})}{E^0_{cell}} \;=\; C_1 \cdot exp(-C_2 \cdot E^0_{cell}/V_{cell}) \;+\; C_3 \right\}_{EMC/HAC}$$

$C_1 \;=\; A_1 \cdot exp(-A_2 \cdot E_{jet}) \;+\; A_3 \;+\; A_4 \cdot E_{jet}\;|_{EMC/HAC}$

EMC	A_1=2.1078	A_2=2.6531E-02	A_3=9.5105E-01	A_4=-6.2283E-04
HAC	A_1=2.7096	A_2=7.0390E-02	A_3=8.3998E-01	A_4=-1.5319E-03

$C_2 \;=\; A_1 \cdot exp(-A_2 \cdot E_{jet}) \;+\; A_3\;|_{EMC/HAC}$

EMC	A_1=1.4006	A_2=1.7496E-02	A_3=1.2746E-01
HAC	A_1=6.2154	A_2=2.0000E-02	A_3=2.5000E-01

$C_3 \;=\; A_1 \cdot exp(-A_2 \cdot E_{jet}) \;+\; A_3 \;+\; A_4 \cdot E_{jet}\;|_{EMC/HAC}$

EMC	A_1	A_2	A_3	A_4
θ=10.1°	1.6838E-01	2.6674E-01	9.8840E-01	-6.7813E-05
θ=25.0°	2.4493E-03	2.5730E-01	9.1478E-01	-4.9166E-05
θ=34.3°	-5.8955E-01	4.2233E-03	1.4807	-1.2209E-03
θ=53.5°	-1.0518E-01	3.5156E-02	9.3712E-01	5.8225E-04
θ=79.0°	-8.0190E-01	1.1574E-02	1.5087	-3.1198E-03
HAC	A_1	A_2	A_3	A_4
θ=10.1°	-9.1569E-01	1.1214E-01	1.1702	-2.4113E-04
θ=25.0°	-8.6698E-01	8.1841E-02	1.0322	8.9294E-05
θ=34.3°	-9.1190E-01	7.9990E-02	1.0430	2.0607E-05
θ=53.5°	-7.9295E-01	5.5478E-02	1.2267	-1.6256E-03
θ=79.0°	-8.8128E-01	8.7020E-02	1.1713	-6.7697E-04

Table 5.1: *Energy parametrization of the weighting parameters for jets for the various regions of the calorimeter.*

In the jet energy range from 5 GeV to 250 GeV and for the whole angular range covered by the H1–LAr–Calorimeter, we find a sizable improvement of the energy resolution when we use π^0–weighting. The energy resolution achieved is about $55\%/\sqrt{E}$ for all jet energies and directions. A possible constant term in the energy resolution is not visible.

In order to be able to apply the weighting method for all jet energies and calorimeter regions we parametrized the weighting constants for the various jet directions as a function of the jet energy.

Optimizing all three parameters of one calorimeter part in parallel we found strong and nonregular energy and angular dependencies of the parameters, but also very large correlation (up to 99%) between the weighting parameters. These correlations were exploited, in order to achieve a smooth energy and theta dependence. The results are shown in the figures 5.2 and 5.3. By making use of the correlations it is possible to parametrize four of the six weighting parameters angular independent, without increasing the χ^2 of the fit. The residual two parameters, the asymptotic values of the weighting functions, show angular variations of the size expected from the studies on linear calibration. For all six parameters we obtained a good energy parametrization using the exponential function with a small linear term, already known from the linear

calibration. The resulting functions are given in table 5.1. They are shown ind 5.2 and 5.3 for EMC and HAC respectively.

The energy dependence of the calibration constants is steady, the residual angular dependence is small. Thus it is possible to apply this parametrization in any selfconsistent iterative procedure, that starts from the ideal electromagnetic scale.

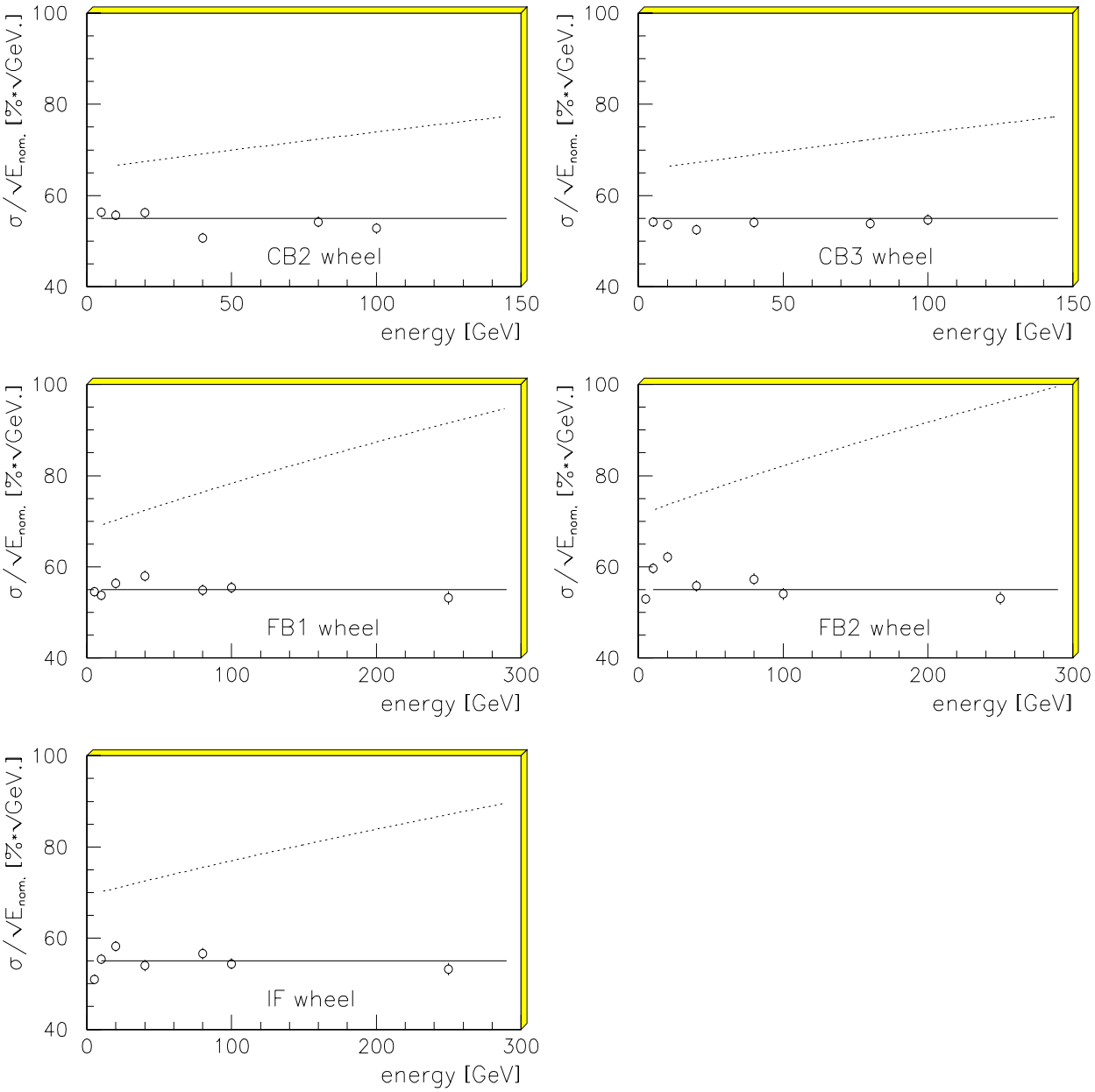

Figure 5.1: *Energy resolution achieved by simultaneous optimization of all six weighting parameters at each individual data point for a 2/4·σ_{noise} topological noise cut and a 3·σ_{noise} energy threshold for weighting as a function of the jet energy in the various calorimeter sections.*

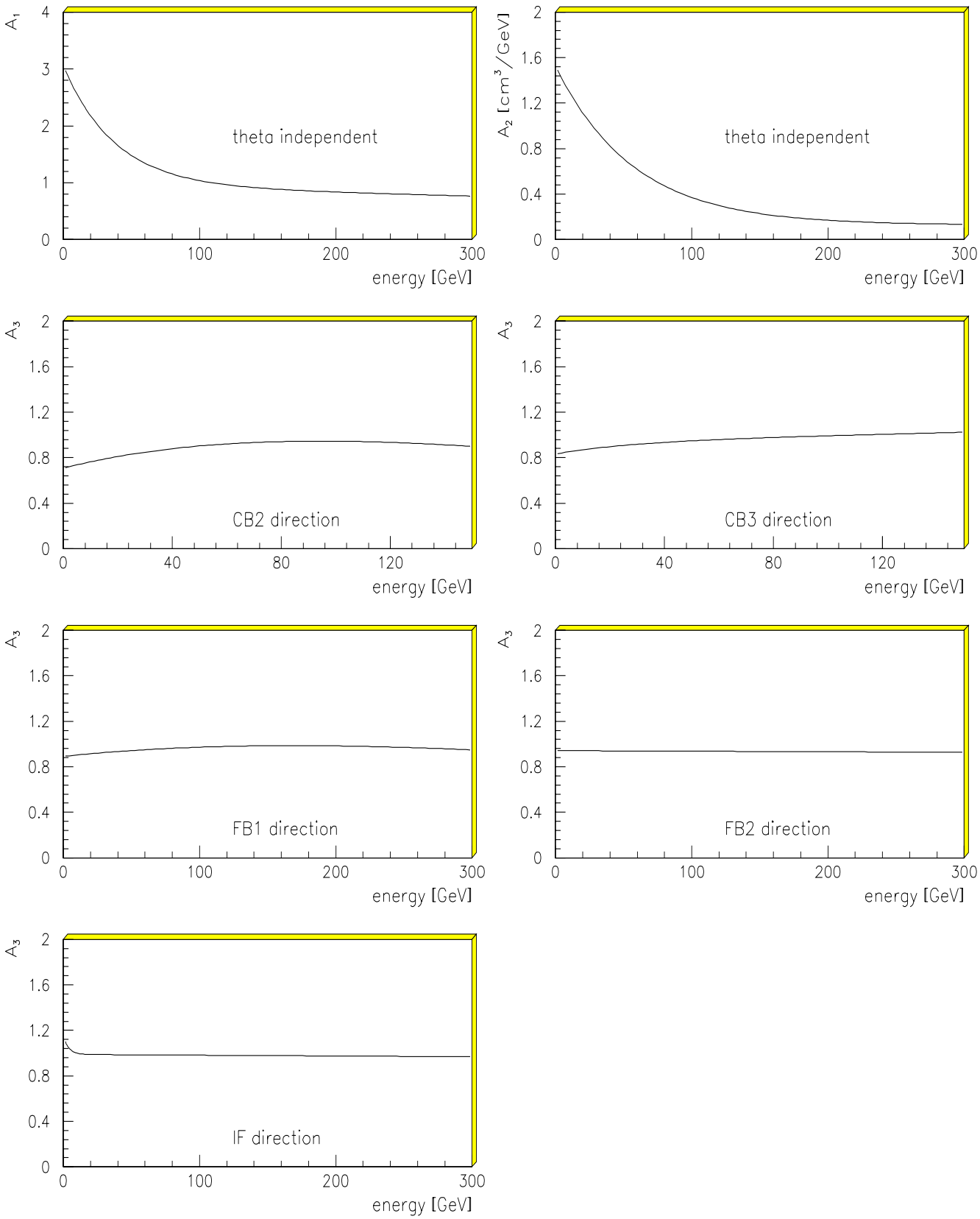

Figure 5.2: *Parametrization of the three weighting parameters of the electromagnetic calorimeter part for a 2/4·σ_{noise} topological noise cut and a 3·σ_{noise} energy threshold for weighting as a function of the jet energy for the various calorimeter regions.*

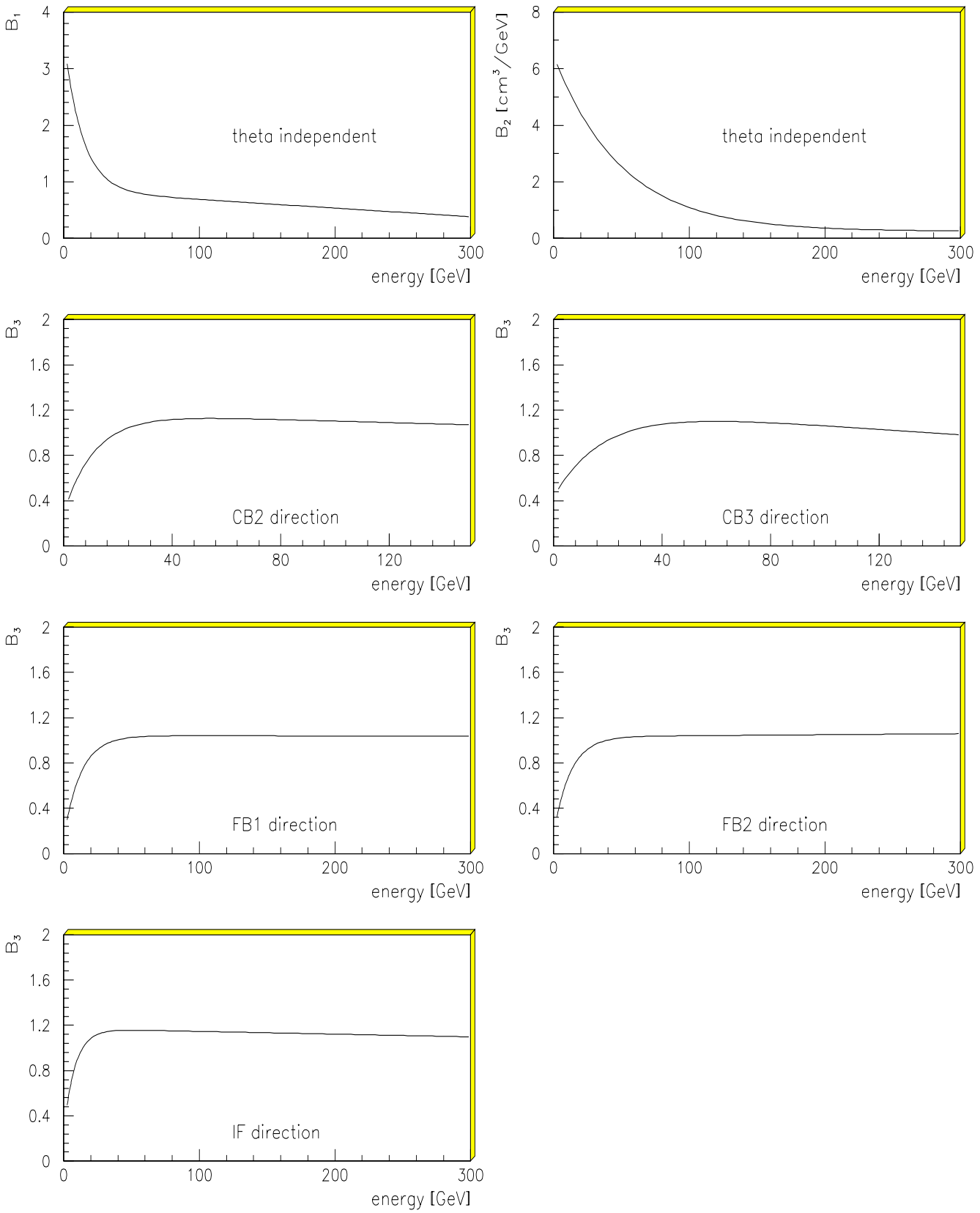

Figure 5.3: *Parametrization of the three weighting parameters of the hadronic calorimeter part for a 2/4·σ_{noise} topological noise cut and a 3·σ_{noise} energy threshold for weighting as a function of the jet energy for the various calorimeter regions.*

5.2 Application of the H1–weighting module for u–quark–jets

$\frac{\sigma}{E} = \sqrt{\frac{A^2}{E} + \frac{B^2}{E^2} + C^2}$					
direction:	CB2E	CB3E	FB1E	FB2E	IFE
A [$\%\sqrt{GeV}$]	55.5	53.3	56.5	57.2	55.0
B [GeV]	0.371	0.175	0.379	0.000	0.000
C [%]	0.00	2.20	0.00	0.00	0.00

Table 5.2: *Contributions to the energy resolution of the H1–LAr–Calorimeter for the various jet directions.*

In order to apply the parametrization of the weighting parameters, we used the cone algorithm described in [Kube94]. Using this procedure, the calibration constants are determined iteratively from the energy of all clusters inside (energy center of gravity) a cone with opening angle α and the cone axis. The cone axis is defined by the line from the nominal interaction vertex to the energy center of gravity of all clusters inside the cone. The weighting parameters are then applied for all clusters inside an outer cone with identical cone axis, but a larger opening angle β. The angles α and β are free parameters. It makes sense not to choose β much larger than α.

Both angles have been chosen as small as possible to minimize errors in more–jet–events. The lower limit is given by the requirement that there is no significant influence of the cone algorithm on the absolute energy calibration and resolution. Results for examples of combinations of α and β are shown in 5.4 and 5.5 respectively. The systematic errors of the energy resolution and the absolute energy measurement due to the choice of α are generally small as long as β is large. For fixed α the energy resolution is degraded with decreasing β. From the request, that the change of the measured energy due to the cone algorithm is smaller than 2% for all calibration points and a minimal degradation of the energy resolution, we obtain α=10° and β=11°. These values are used in the following.

In fig. 5.6 we show the energy resolution achieved in this procedure. The dotted line is the resolution obtained with the linear ansatz, the solid line indicates the $55\%/\sqrt{E}$ goal.

The parametrization (equation 3.1) of the energy resolution [Fabian89] was fitted to the data. The various terms are compiled in table 5.2. With the given calibration, we achieve for the H1–LAr–Calorimeter a 'sampling term' of about $55\%\sqrt{GeV}$. A constant term is not observed, except for the CB3 direction, where we find a constant contribution to the energy resolution of 2.2%.

Fig. 5.7 shows the quality of the absolute energy measurement. The $\pm 1\%$ and $\pm 2\%$ lines are indicated.

The precision of the absolute energy measurement for almost all directions and energies is better than 1% at the calibration points. Only for the lowest energies we see somewhat larger deviations. The largest difference between measured and deposited energy (4%) is found for 5 GeV jets in IF direction.

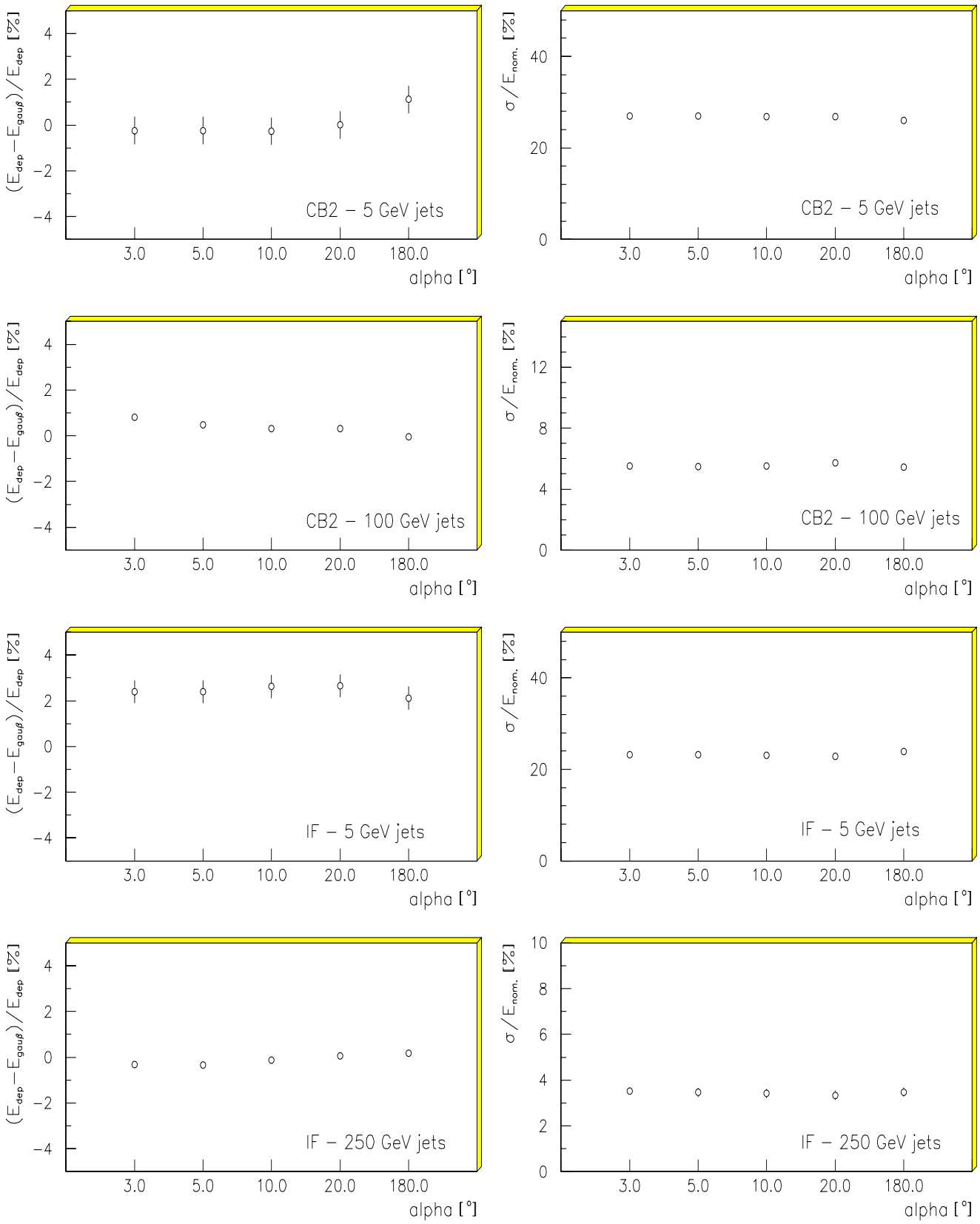

Figure 5.4: *Energy resolution and relative difference of reconstructed and deposited energy as a function of the cone opening angle α for an outer cone opening angle $\beta =$ 180°.*

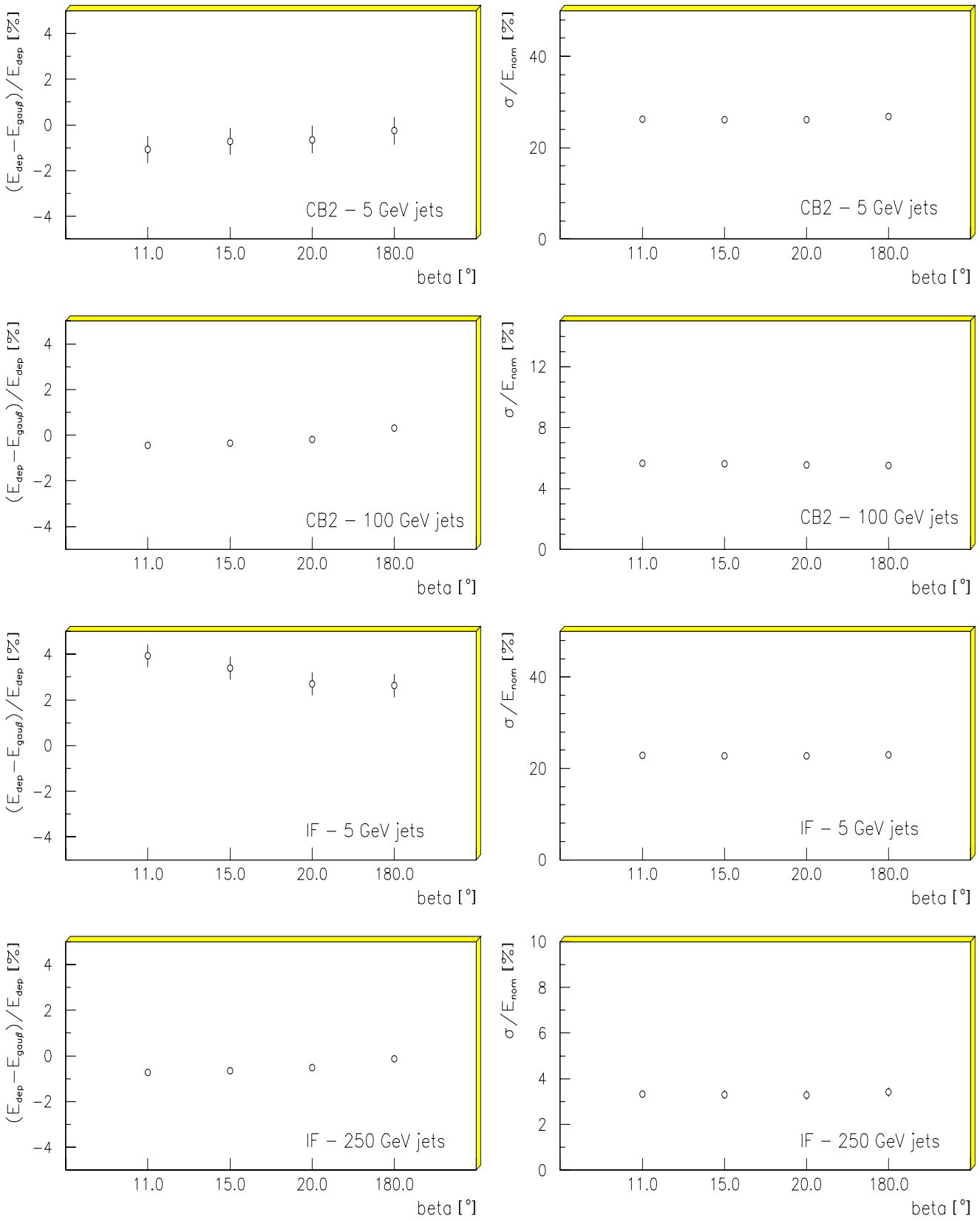

Figure 5.5: *Energy resolution and relative difference of reconstructed and deposited energy as a function of β for a inner cone opening angle $\alpha = 10°$.*

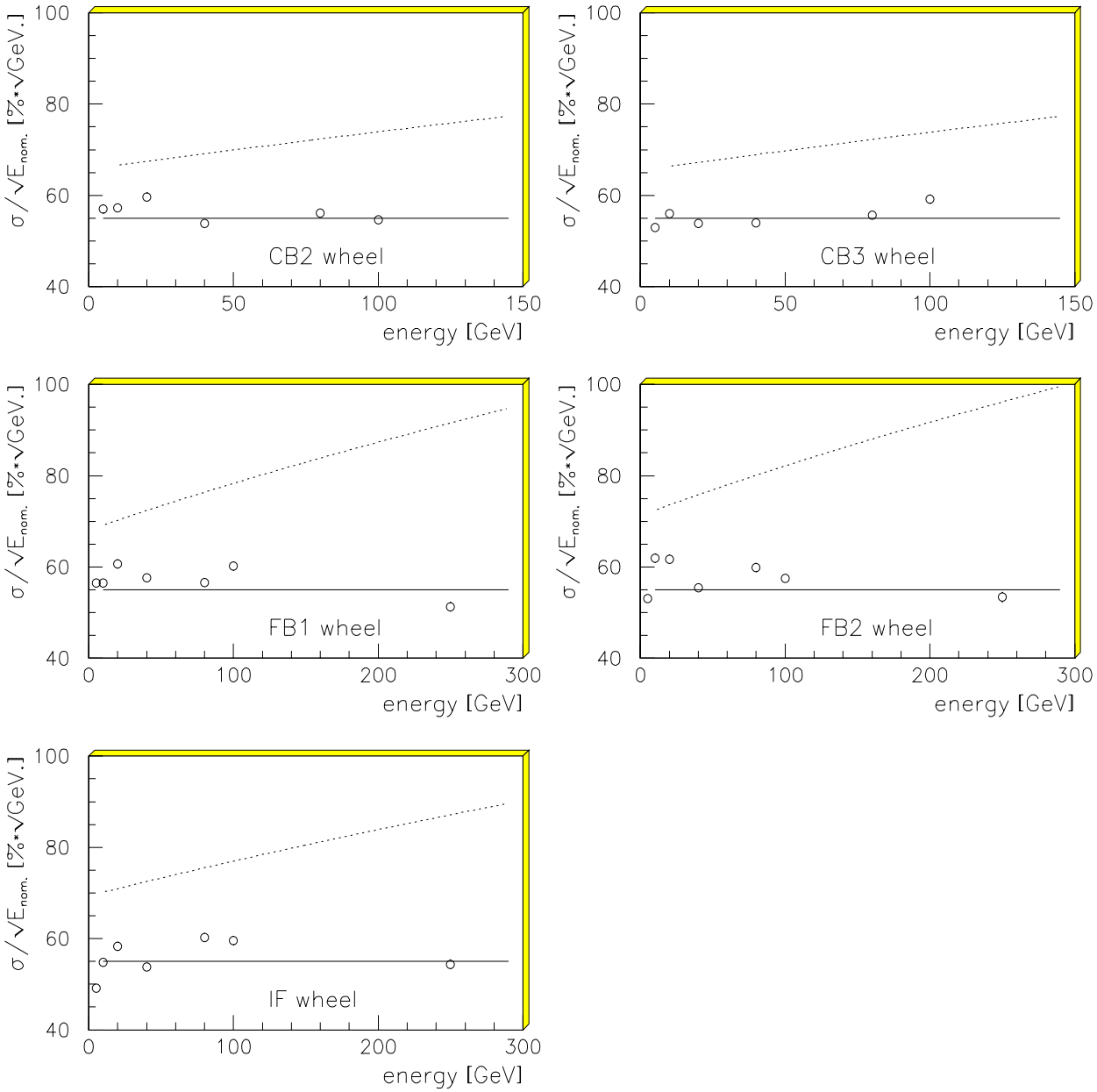

Figure 5.6: *Energy resolution found in the various calorimeter regions by applying the given parametrization of the weighting parameters to jet data from the calibration matrix points using the cone algorithm.*

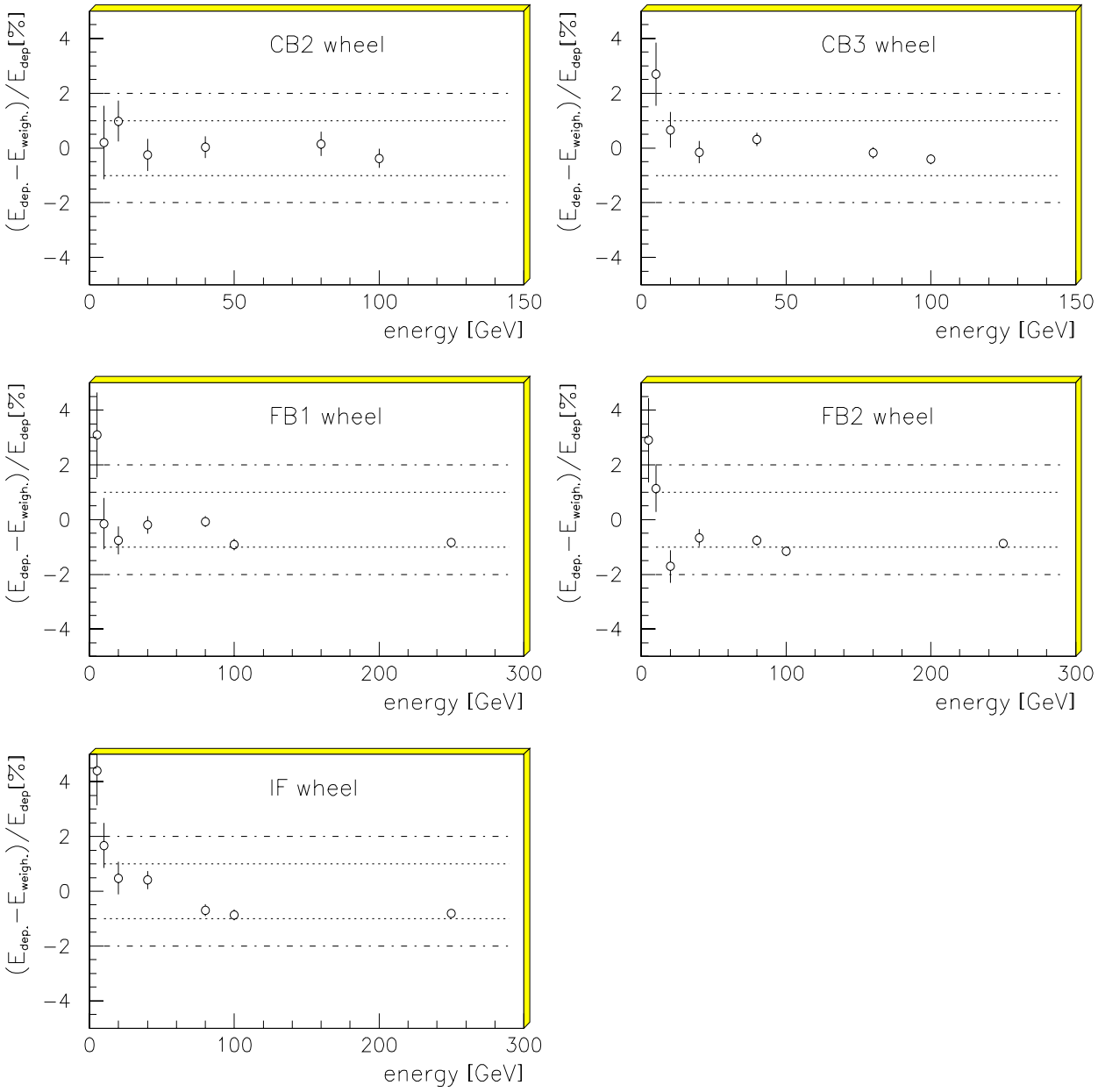

Figure 5.7: *Relative difference of reconstructed and deposited energy in the various calorimeter regions found by applying the given parametrization of the weighting parameters to jet data from the calibration matrix points using the cone algorithm.*

5.3 Systematic studies on the quality of the hadronic calibration

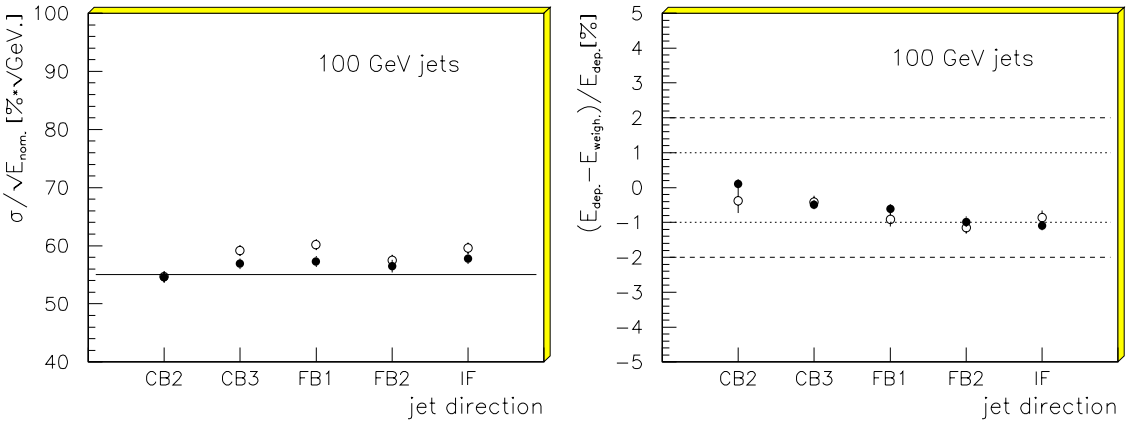

Figure 5.8: *Energy resolution and relative difference of reconstructed and deposited energy in the various calorimeter regions found by applying the given parametrization of the weighting parameters to jet data at calibration matrixpoints using the cone algorithm. The data were not used in the optimization of the weighting parameters.*

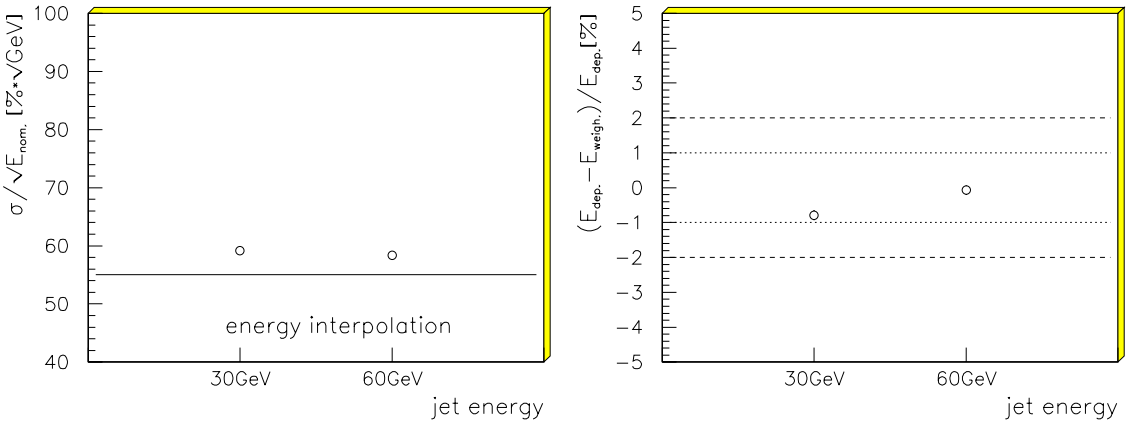

Figure 5.9: *Energy resolution and relative difference of reconstructed and deposited energy found when applying the given parametrization of the weighting parameters for jet data at $\theta = 34.3°$, which is the FB1 calibration matrix direction, at energies not used in the determination of the weighting parameters.*

In the following we will present results on the statistical representativity of the data samples used for calibration, the quality of the energy interpolation, the quality of the theta interpolation (and extrapolation) and the particle type dependence of the hadronic energy measurement.

Statistical representativity of the calibration data

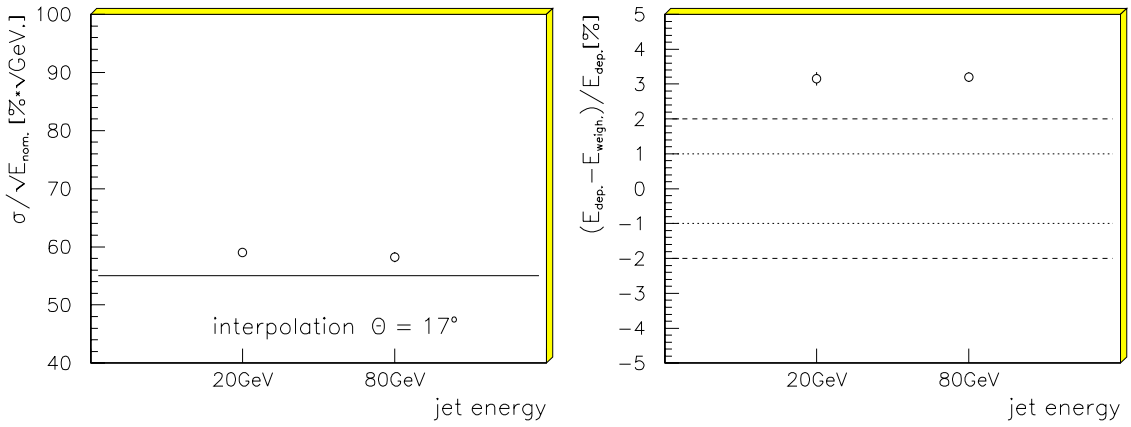

Figure 5.10: *Energy resolution and relative difference of reconstructed and deposited energy found when applying the given parametrization of the weighting parameters for jets at a jet angle of* $\theta = 17°$ *and energies at calibration matrix points.*

We simulated u–quark–jets at 100 GeV energy for the various jet directions, 2000 events at each theta point. These data are on calibration points, but were not used for the optimization of the weighting parameters. Applying the given calibration to these data we check the statistical representativity of the calibration data.

Fig. 5.8 shows the results on energy resolution and absolute energy measurement (full points) together with those found for the calibration data (open circles). The results on absolute energy measurement found for the two samples are consistent within errors. Despite of the fact, that identical automatical fit procedures were employed for the calculation of the energy resolutions, the resolution tends to be better for the data that were not used in the calibration. The data samples used for calibrating the hadronic response of the H1–LAr–Calorimeter are statistically representativ at the 0.1% level for absolute energy measurement, and at the $1.5\%\sqrt{E}$ level for energy resolution.

quality of the energy interpolation

In order to estimate systematic errors due to the energy interpolation of the calibration constants, we simulated jets at 30 GeV and 60 GeV energy in direction of the FB1–calibration point, 4000 events each. The results found when applying the calibration to these data are shown in fig. 5.9. We find energy resolutions between $55\%/\sqrt{E}$ and $60\%/\sqrt{E}$. The error on the absolute energy measurement is smaller than 1%. The results are competeable to what has been found for calibration data.

The energy interpolation does not lead to any sizable degradation of energy resolution and absolute energy measurement.

Quality of the angular inter/extrapolation

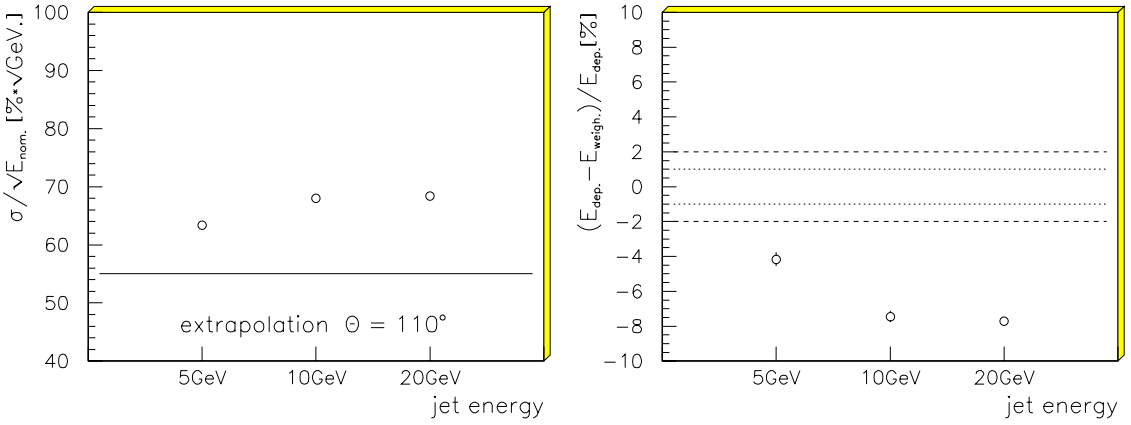

Figure 5.11: *Energy resolution and relative difference of reconstructed and deposited energy found when applying the given parametrization of the weighting parameters for jets with a jet angle of* $\theta = 110°$ *and energies at calibration matrix points.*

In order to investigate systematic effects due to the use of the theta inter/extrapolation of the weighting parameters for fixed jet energy, we simulated jets at an polar angle of $\theta = 17°$ for 20 GeV and 80 GeV jet energy and at $\theta = 110°$ for 5 GeV, 10 GeV and 20 GeV jet energy, 4000 events each. The results found by applying the calibration to these data are shown in the figures 5.10 and 5.11. For the theta interpolation of the calibration constants we find a systematic error of the absolute energy measurement of 3%, independent of the jet energy. The energy resolution $\sigma/\sqrt{E}$ is found to be $59\%/\sqrt{E}$, which is consistent with the resolution found at the calibration points.

For angles larger than 79.0° in the given cheme the weighting parameters found for the CB2 direction are applied. In this region ($\theta = 110°$) the mean reconstructed energy is found to be too large by up to 7%. The energy resolution is degraded by approximately 7%, too.

Test of the particle type dependence of the hadronic energy measurement

The particle type dependence of the energy reconstruction was tested using selected jet data with large primary electromagnetic content, f_{em}. We selected jets with $f_{em} > 60\%$ and $f_{em} > 80\%$.

The quality of the absolute energy calibration is shown in the figures 5.12 and 5.13. In the case of $f_{em} > 60\%$ for all jet energies greater than 5 GeV the mean relative difference between reconstructed energy and deposited energy is smaller than 1%, except for the FB direction, where we found 2% at maximum. For the 5 GeV data the difference between the mean reconstructed and the mean deposited energy is typically -4%. In the case of $f_{em} > 80\%$ the data statistic is sufficient only for high jet energies. Here systematic errects on the absolute energy measurement are smaller than 1.3% in all cases.

In conclusion, the calibration given is independent of the individual composition of the jets at the required level. One of the major goals of the hadronic calibration was achieved. After calibration the signals of electrons and hadrons are identical. The H1–LAr–Calorimeter is (software)compensating after weighting.

The energy resolution, $\sigma/\sqrt{E}$, found for high f_{em} jets is shown in fig. 5.14 and 5.15 (full points). For $f_{em} > 60\%$ we show in addition the resolution obtained with linear calibration (dotted line) and with weighting without preselecting high f_{em} jets (open circles). The solid line corresponds to $55\%\sqrt{GeV}$. In the case of $f_{em} > 80\%$ instead of the resolutions found for weighting without selection of high f_{em} jets we show the results found for $f_{em} > 60\%$.

The energy resolution is significantly improved after in the selection. For $f_{em} > 60\%$ we found a resolution of $40\%\sqrt{GeV}$ to $45\%\sqrt{GeV}$. For the $f_{em} > 80\%$–jet sample the energy resolution is further improved by about $15\%\sqrt{GeV}$, reaching the $25\%\sqrt{GeV}$ to $35\%\sqrt{GeV}$ range. For large data statistic and sufficient understanding of the systematic effects, this strong improvement of the energy resolution will be very valuable for reconstructing the kinematic of individual events. A f_{em} preselection (for the current jet) will result in an impressive improvement of the precision of the energy measurement in the hadronic final state.

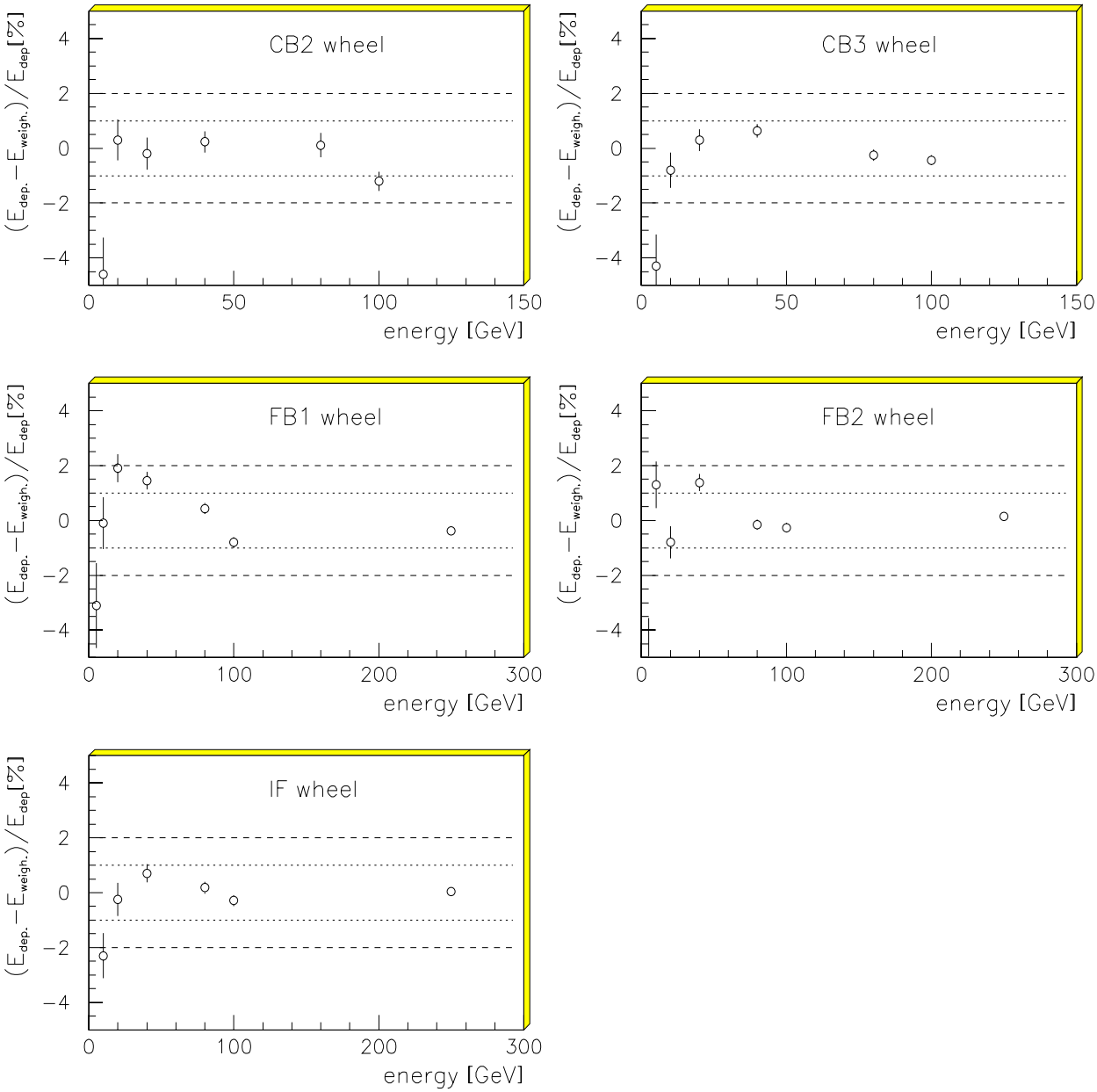

Figure 5.12: *Relative difference of reconstructed and deposited energy in the various calorimeter regions. The data used are preselected jets with a primary electromagnetic fraction larger than 60 %. The* $\pm$ 1% *and* $\pm$ 2% *lines are indicated.*

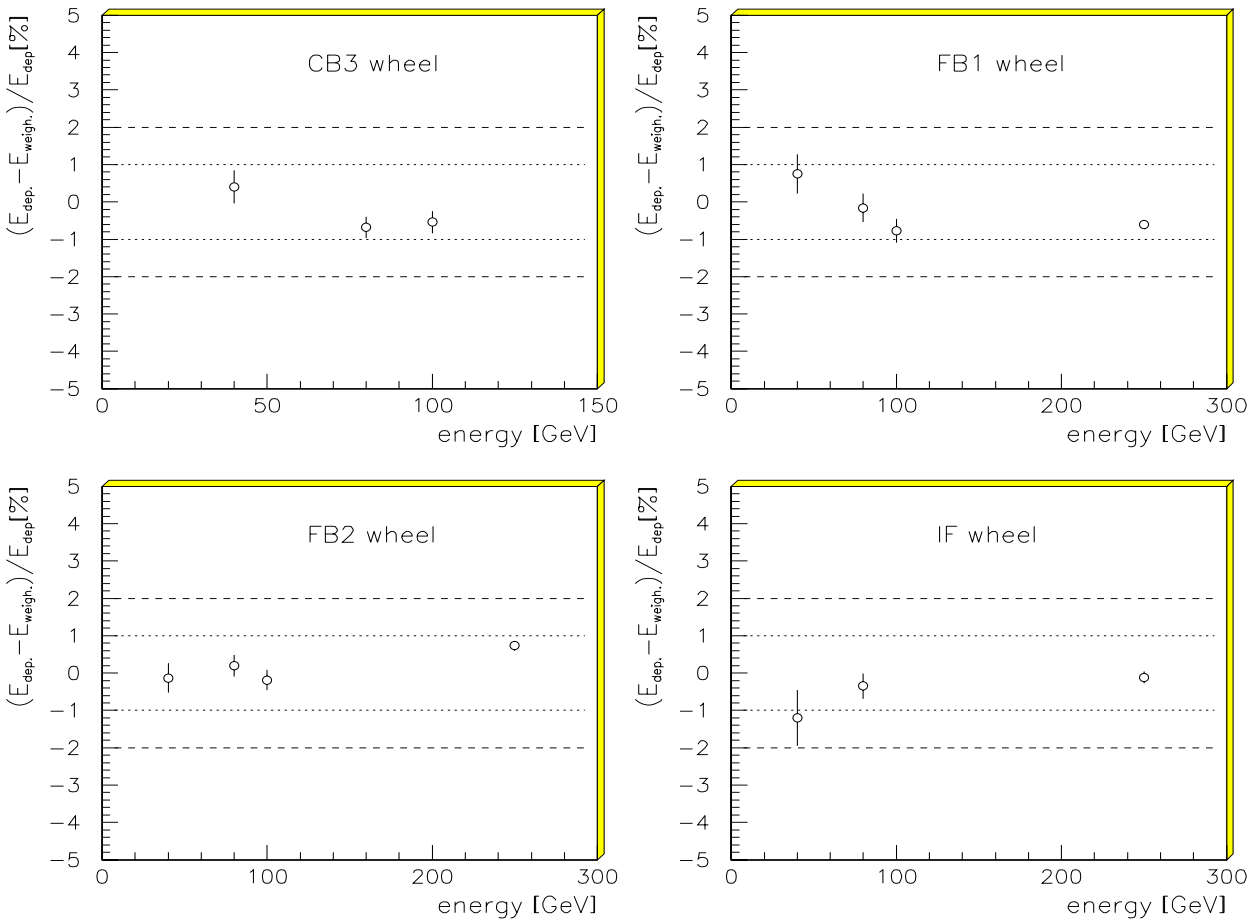

Figure 5.13: *Relative difference of reconstructed and deposited energy found in the various calorimeter regions. The data used are preselected jets with a primary electromagnetic fraction larger than 80 %. The* $\pm$ 1% *and* $\pm$ 2% *lines are indicated.*

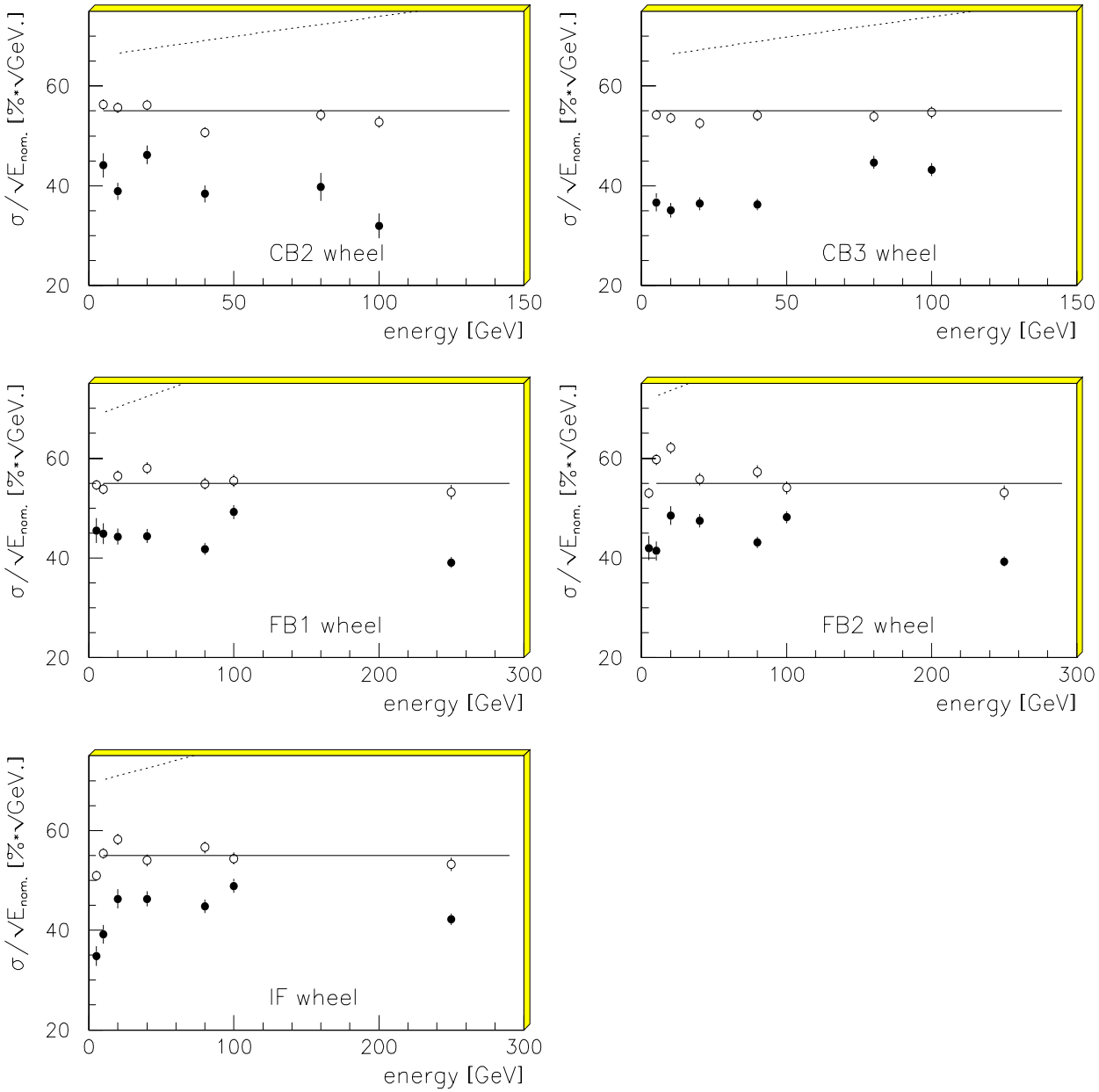

Figure 5.14: *Energy resolution found in the various calorimeter regions. The data used (full points) are preselected jets with an primary electromagnetic fraction larger than 60%. The open circles show the energy resolution achieved for all jets The goal (full line) and the energy resolution achieved with the linear calibration ansatz (dotted line) are indicated.*

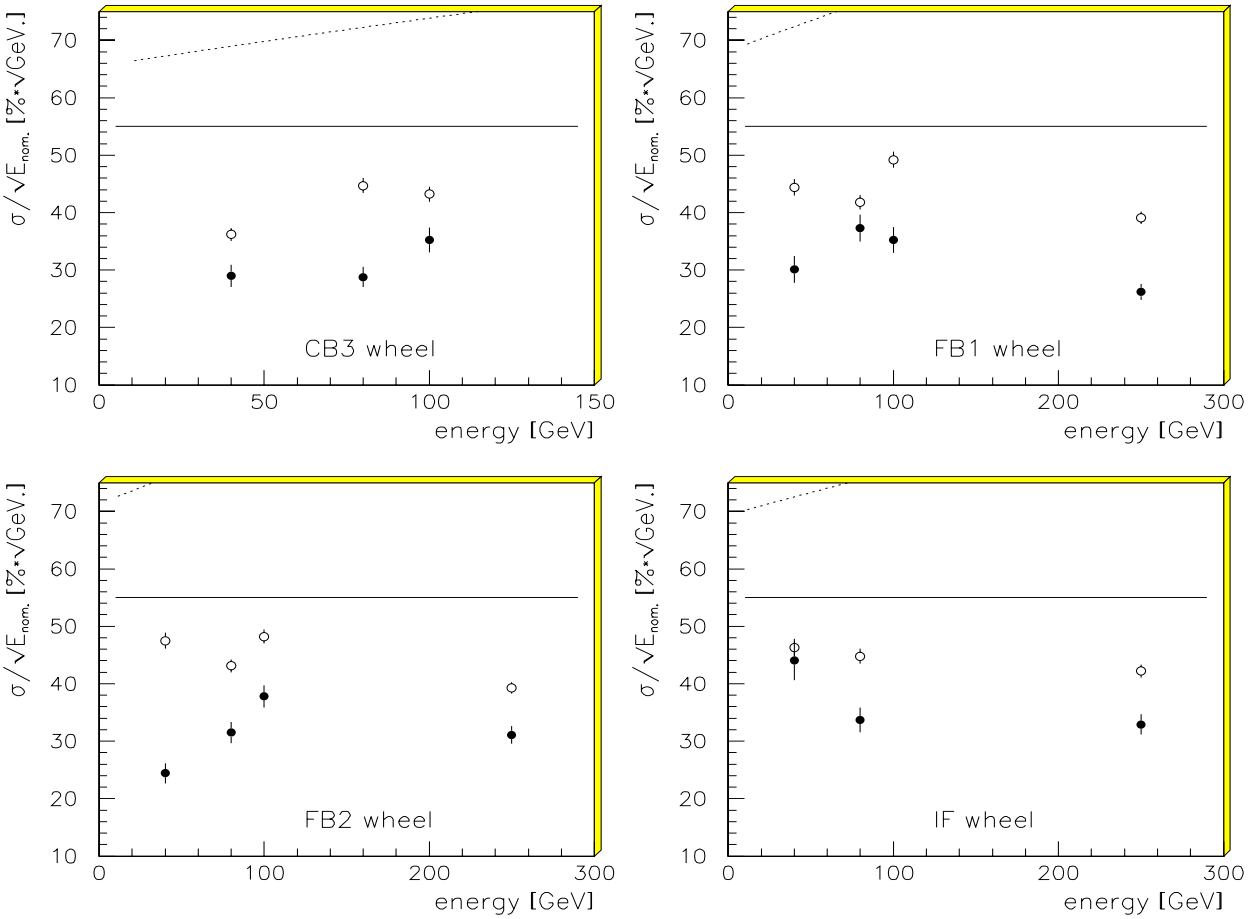

Figure 5.15: *Energy resolution found in the various calorimeter regions. The data used (full points) are preselected jets with an primary electromagnetic fraction larger than 80 %. The open circles show the energy resolution achieved for preselected jets with an primary electromagnetic fraction larger than 60 %. The goal (full line) and the energy resolution achieved with the linear calibration ansatz (dotted line) are indicated.*

6. Weighting including an estimation of the electromagnetic content of jets

It has been shown in [Greiff90], that it is possible to significantly improve the hadronic energy resolution in the H1–LAr–Calorimeter by estimating the primary electromagnetic content of hadronic cascades and including this information in the weighting ansatz explicitly. The improvement found in $\sigma/\sqrt{E}$ was about $5\%\sqrt{\mathrm{GeV}}$ to $10\%\sqrt{\mathrm{GeV}}$.

In the following we further investigate this possibility. We will present a method, that allows to estimate efficiently the energy deposited in the electromagnetic calorimeter by electromagnetic showers in all calorimeter regions and for all available jet energies. Furthermore we investigate to which extent the improvement of the energy resolution seen in [Greiff90] depended on the use of monte carlo quantities in the estimation of the electromagnetic fraction.

In the following the electromagnetic fraction of a jet is defined as the ratio of the energy of the jet deposited in the electromagnetic calorimeter by electrons, positrons and photons (which is to be estimated) to the total energy deposited in the calorimeter.

$$f_{em} \;=\; \frac{E^{em}_{estimate}}{E_{normalisation}}$$

The following weighting ansatz has been used[Kube94]:

$$\left\{ \frac{E_{cell}(E^0_{cell})}{E^0_{cell}} \;=\; 1 \;+\; (1-f_{em})\cdot\Big(C_1\cdot exp\{-C_2\cdot(1-f_{em})\cdot E^0_{cell}/V_{cell}\} \;+\; C_3\Big)\right\}_{EMC/HAC}$$

The parameters C_1, C_2 and C_3 are optimized for EMC and HAC independently in the minimum χ^2 fit described in chapter 2.

In the case of $f_{em} = 1$ this ansatz returns the ideal electromagnetic scale. For decreasing f_{em} the influence of the weighting part of the ansatz increases. At the same time the exponential form of the weighting part becomes steeper and more pronounced.

In the analysis all methods concerning noise cut, preselection of electromagnetic showers, etc. have been applied as described in the preceding chapter.

Estimation of the electromagnetic energy content of a jet, $E^{em}_{estimate}$

In order to estimate the energy, that was deposited by electromagnetic showers in the electromagnetic calorimeter part, we used the criteria developed for particle identification, EAK0 and EAH4 [Sirois93], already employed in the preselection of electromagnetic showers. In our method the sum over the energies of all clusters obeying the following conditions is used as an estimate:

- The cluster energy is larger than 100 MeV.
- The cluster consists of at least two calorimeter cells.
- More than 97% of the cluster energy is reconstructed in the EMC.
- At least one of the criteria EAK0 or EAH4 is obeyed for an electron identification efficiency of 99%.
- The cluster energy center of gravity is not closer to a ϕ–crack than 44 mrad.

Using these conditions we obtained reasonable results for all jet directions and energies. As an example we show in fig. 6.1 for the CB2 direction and the various jet energies the correlation of the energy deposited in EMC by electromagnetic showers and the corresponding estimate. The quality of the correlation is similar for all other calorimeter regions.

Estimate of the total energy deposited by the jets, $E_{normalisation}$

In order to normalize the electromagnetic fraction we used three different quantities:

1. In analogy to [Greiff90] a monte carlo quantity, the total energy deposited in the calorimeter, E^{MC}_{dep}, was used.
2. The total reconstructed energy, E_{rec}, using the calibration given in chapter 5 was used. This method does not involve any MC quantity.
3. The total energy deposited in the calorimeter (MC) smeared with the energy resolution obtained with the calibration described in chapter 5, $E^{MC,smeared}_{dep}$, was used.

Method 2. is the only one, that could possibly be applied to real data.

Discussion of the achievable energy resolution

In the figs. 6.2, 6.3 and 6.4 we show the energy resolution obtained by using the three ways to normalize the electromagnetic fraction (full points) together with the resolution obtained with the usual exponential weighting function, i.e. without estimation of the electromagnetic fraction.

In case 1., using the pure monte carlo normalisation, we found an improvement of the

energy resolution by the amount expected from the previous work [Greiff90]. The effect is seen for all energies and jet directions. In case 2., where we use only reconstructed quantities, this improvement of the energy resolution is not observed. After a gaußian smearing of the monte carlo normalisation by the experimental energy resolution, case 3., we see a slight improvement of the energy resolution in CB2 direction. For all other jet directions we do not see any improvement of the energy resolution. The excellent result seen in case 1. is not reproduceable.

An improvement of the energy resolution by using the procedure described in [Greiff90], i.e. by estimating the electromagnetic fraction of a jet and using it explicitely in the weighting ansatz, seems not possible when using reconstructed quantities only. The effect described there appears to be predominantly due to the at that time unavoidable use of monte carlo quantities.

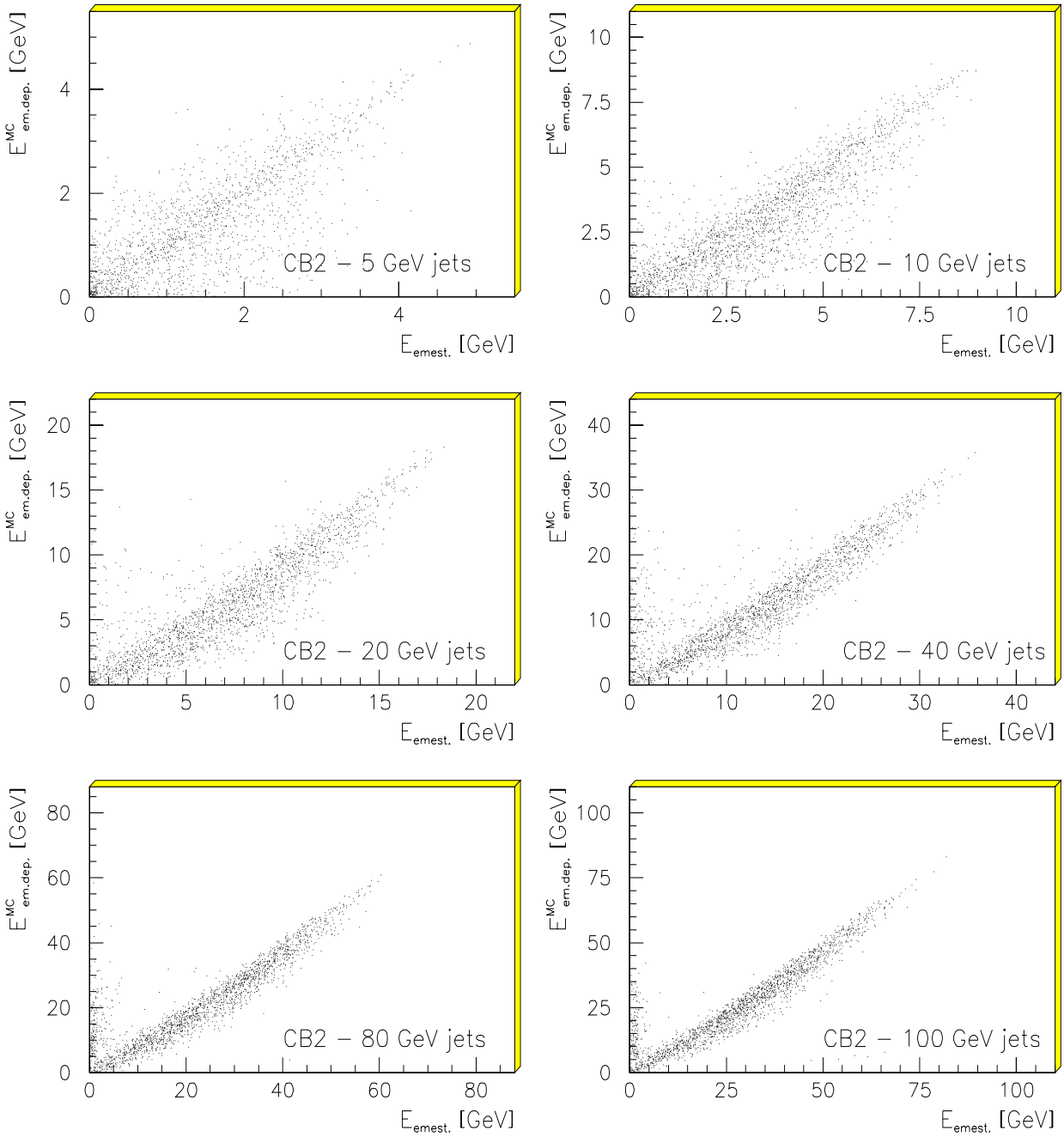

Figure 6.1: *Correlation of the total energy deposited in the electromagnetic calorimeter by electrons, positrons and photons (this includes parts of the electromagnetic fraction of hadronic showers starting in the EMC) and the corresponding estimate for the various jet energies in CB2 direction.*

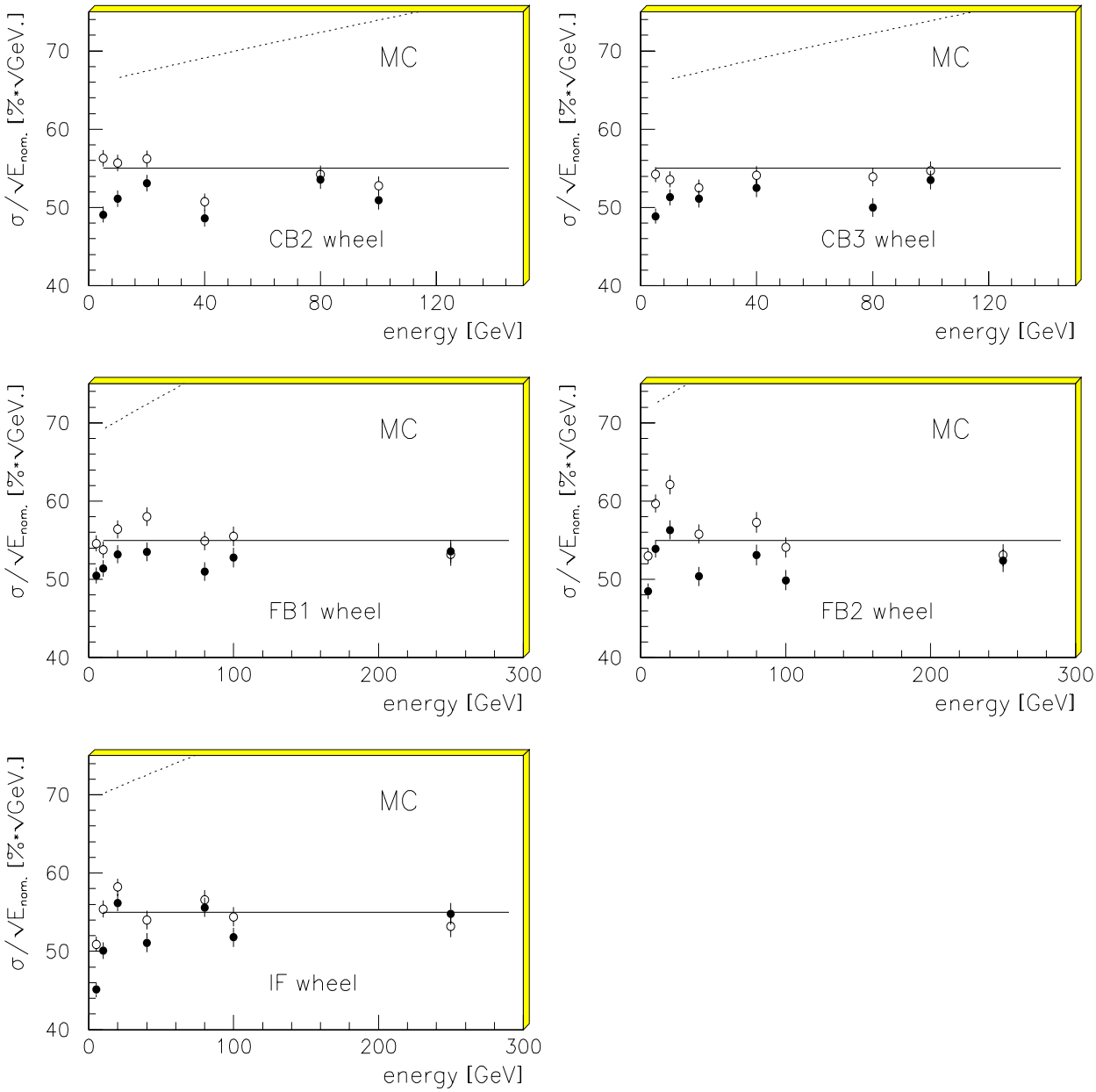

Figure 6.2: *The full points show the energy resolution obtained using the estimation of the electromagnetic fraction of a jet:* $f_{em} = E^{MC}_{estim.}/E^{MC}_{dep.}$*; i.e. using MC information in analogy to [Greiff90]. The open circles show the energy resolution obtained with the weighting ansatz without estimation of the electromagnetic fraction of the jets. The full and the dotted line indicate the goal resolution and the energy resolution obtained with a linear calibration ansatz respectively.*

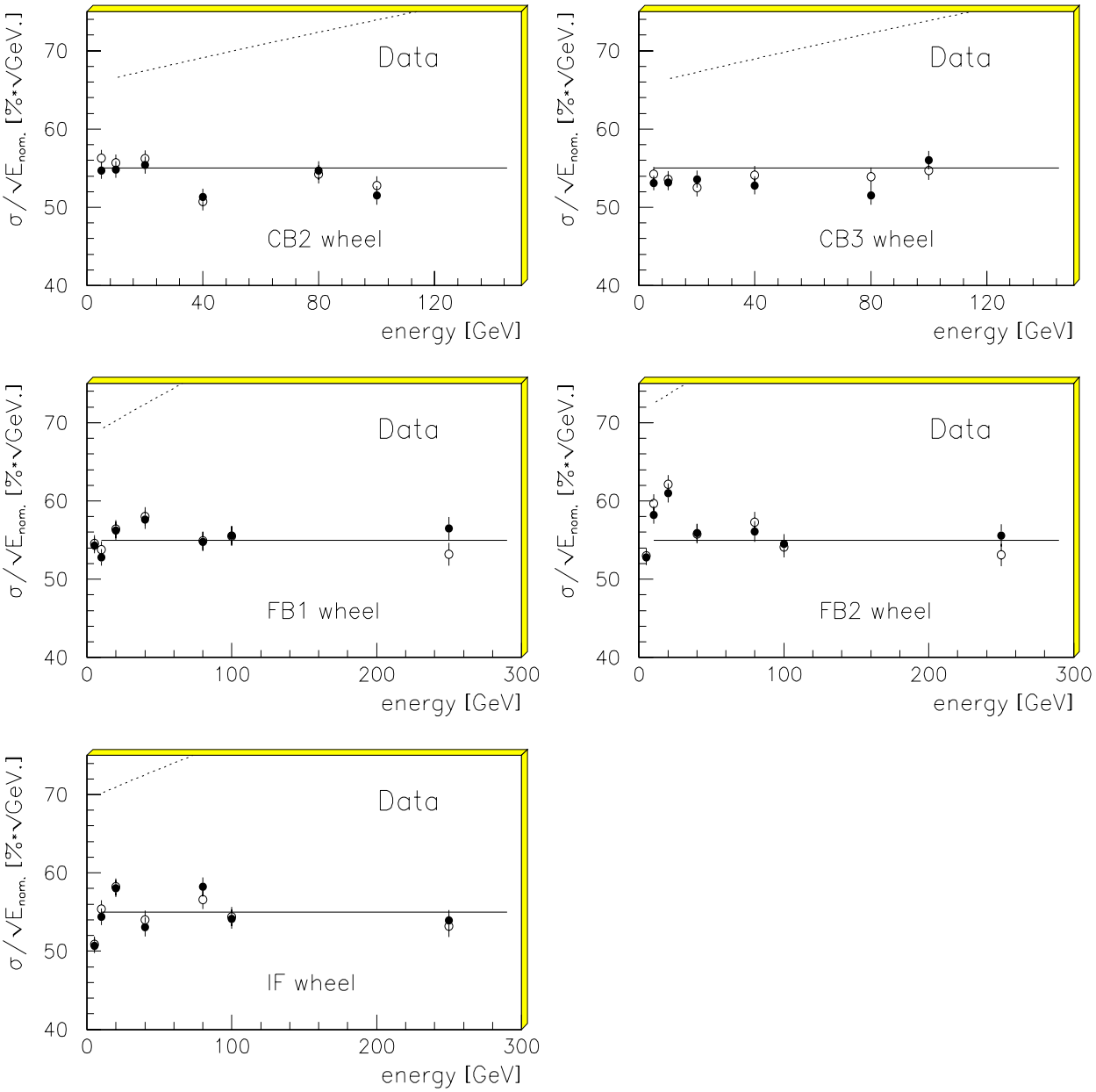

Figure 6.3: *The full points show the energy resolution obtained using the estimation of the electromagnetic fraction of a jet:* $f_{em} = E^{MC}_{estim.}/E_{rec.}$*; i.e: Without using any MC information.* E_{rec} *is the energy reconstructed with the given parametrization of the weighting parameters for each individual jet. The open circles show the energy resolution obtained with the weighting ansatz without estimation of the electromagnetic fraction of the jets. The full and the dotted line indicate goal resolution and the energy resolution obtained with a linear calibration ansatz respectively.*

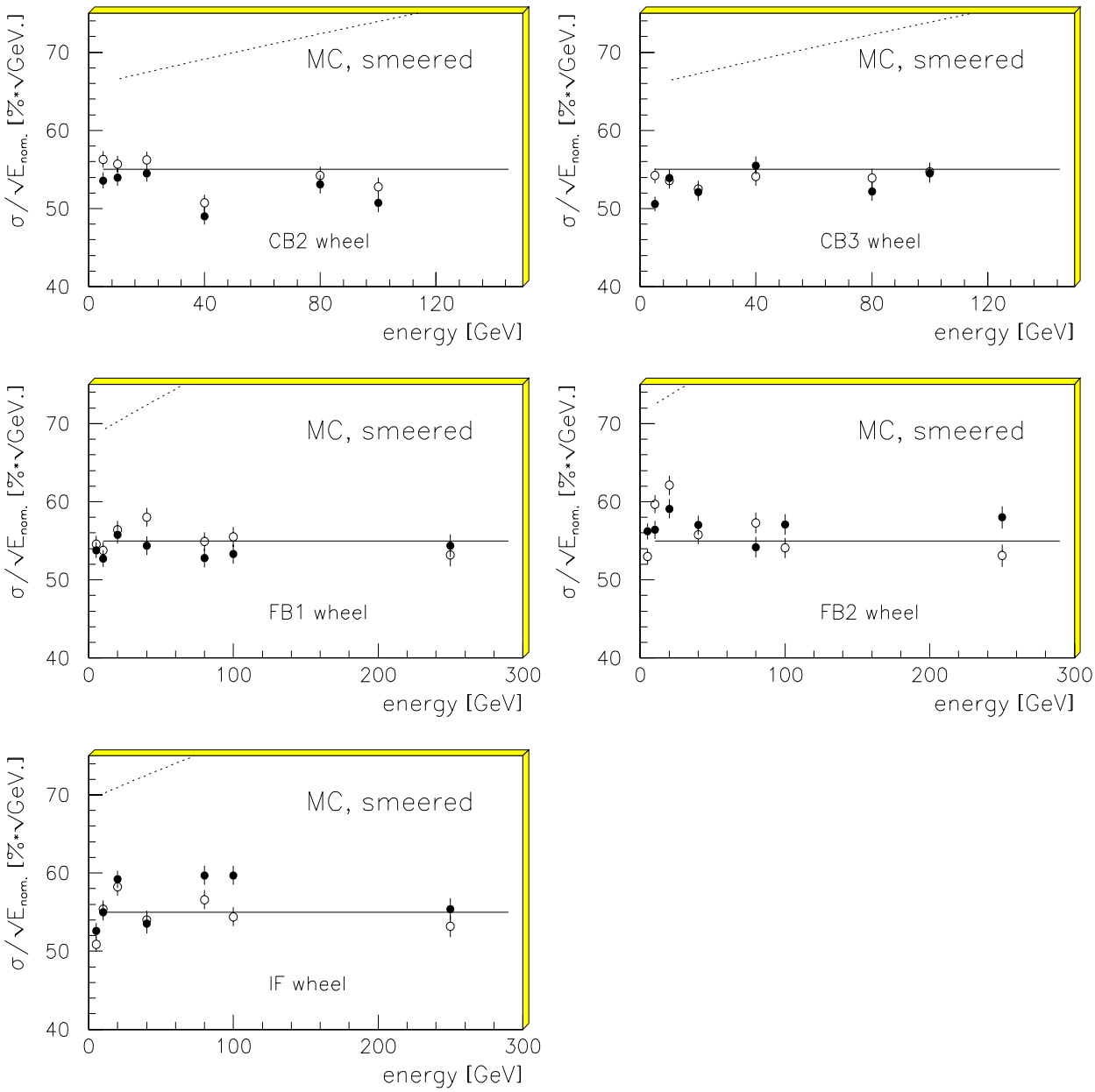

Figure 6.4: *The full points show the energy resolution obtained using the estimation of the electromagnetic fraction of a jet:* $f_{em} = E^{em}_{estim.}/E^{MC,smeered}_{dep}$*; i.e.: Using MC information, but applying a gaußian smeering to the MC energy using the experimental resolution found for each individual jet energy when applying the parametrisation of the weighting parameters given previously. The open circles show the energy resolution obtained with the weighting ansatz without estimation of the electromagnetic fraction of the jets. The full and dotted line indicate the goal resolution and the energy resolution obtained with a linear calibration ansatz respectively.*

List of Figures

1.1 Energy distribution (energy measurement on the electromagnetic scale) for 80 GeV jets in FB2 direction. The full line is a gauß'ian fit to the distribution. 2

3.1 Calibration parameters (linear calibration) in the electromagnetic calorimeter part for the various jet directions as a function of the jet energy. . . 8

3.2 Calibration parameters (linear calibration) in the hadronic calorimeter part for the various jet directions as a function of the jet energy. 9

3.3 Calibration parameters (linear calibration) in the electromagnetic calorimeter part for various jet energies as a function of jet direction. 10

3.4 Calibration parameters (linear calibration) in the hadronic calorimeter part as a function of jet direction for various jet energies. 11

3.5 Energy resolution achieved in the various calorimeter regions as a function of the jet energy, using linear calibration. The dashed curve is a parametrization of the energy resolution for jet energies larger than 5 GeV, the full line is the goal resolution. 12

4.1 Mean efficiency of the preselection of electromagnetic showers for the various calorimeter regions as a function of jet energy, using the given preselection method. The low values at 5 GeV jet energy are due to a 1 GeV cluster energy cutoff in the preselection. The decrease towards high energy is due to the decrease of the jet opening angle. 17

4.2 Mean fraction of misidentified hadronic energy in the various calorimeter regions as a function of jet energy using the given preselection method. It will be shown, that this misidentification rate is small enough, that no deterioration of the hadronic energy resolution is observed. 18

4.3 Distribution of the efficiency of the preselection of electromagnetic showers, f_{tag}, and the fraction of hadronic energy wrongly classified as electromagnetic, f_{fake}, for the example of 40 GeV jets in CB2 direction and 100 GeV jets in FB2 direction for the preselection procedure used in calibrating the hadronic response of the H1–LAr–Calorimeter. 19

4.4 Energy resolution obtained in the various calorimeter regions using linear calibration, shown as a function of the jet energy (full points). In addition we show the energy resolution obtained when applying the given preselection method (open circles). 25

4.5 Typical energy resolution and mean reconstructed energy as found on the electromagnetic scale for selected jet directions and energies as a function of the noise cut. 26

4.6 Energy resolution normalized to the resolution found for a $2/4 \cdot \sigma_{noise}$ noise cut as a function of the noise cut applied in the optimization of the calibration parameters. The open circles show the behaviour expected from the noise cut dependence of the energy measurement on the electromagnetic scale. 27

4.7 Energy resolution and mean reconstructed energy as a function of the noise cut. As reference point we used the values found for a $2/4 \cdot \sigma_{noise}$ noise cut. The open circles show the results obtained when applying the weighting parameters optimized for a $2/4 \cdot \sigma_{noise}$ cut. The stars show the behaviour of the energy measured on the electromagnetic scale, the full points show the results found when optimizing weighting parameters for each noise cut individually. 28

4.8 Noise signal on the electromagnetic scale summed over the entire LAr–calorimeter as a function of the noise cut. 29

4.9 Enhancement of the noise signal in the weighting procedure as a function of the noise cut for random triggers from H1 cosmic runs and for NC events. 29

4.10 Energy resolution achieved as a function of the energy threshold. Weighting was applied only for cells with energies above the threshold. 30

4.11 Enhancement of the noise energy as a function of the energy threshold for weighting. After a $2/4 \cdot \sigma_{noise}$ noise cut the weighting parameters applied for random and NC events were optimized for each threshold value individually. Only cells above the threshold were considered in the weighting procedure. Cells below the threshold were kept on the electromagnetic scale. 31

5.1 Energy resolution achieved by simultaneous optimization of all six weighting parameters at each individual data point for a $2/4 \cdot \sigma_{noise}$ topological noise cut and a $3 \cdot \sigma_{noise}$ energy threshold for weighting as a function of the jet energy in the various calorimeter sections. 35

5.2 Parametrization of the three weighting parameters of the electromagnetic calorimeter part for a $2/4 \cdot \sigma_{noise}$ topological noise cut and a $3 \cdot \sigma_{noise}$ energy threshold for weighting as a function of the jet energy for the various calorimeter regions. 36

5.3 Parametrization of the three weighting parameters of the hadronic calorimeter part for a $2/4 \cdot \sigma_{noise}$ topological noise cut and a $3 \cdot \sigma_{noise}$ energy threshold for weighting as a function of the jet energy for the various calorimeter regions. 37

5.4 Energy resolution and relative difference of reconstructed and deposited energy as a function of the cone opening angle α for an outer cone opening angle $\beta = 180°$. 40

5.5 Energy resolution and relative difference of reconstructed and deposited energy as a function of β for a inner cone opening angle $\alpha = 10°$. 41

5.6 Energy resolution found in the various calorimeter regions by applying the given parametrization of the weighting parameters to jet data from the calibration matrix points using the cone algorithm. 42

5.7 Relative difference of reconstructed and deposited energy in the various calorimeter regions found by applying the given parametrization of the weighting parameters to jet data from the calibration matrix points using the cone algorithm. 43

5.8 Energy resolution and relative difference of reconstructed and deposited energy in the various calorimeter regions found by applying the given parametrization of the weighting parameters to jet data at calibration matrixpoints using the cone algorithm. The data were not used in the optimization of the weighting parameters. 44

5.9 Energy resolution and relative difference of reconstructed and deposited energy found when applying the given parametrization of the weighting parameters for jet data at $\theta = 34.3°$, which is the FB1 calibration matrix direction, at energies not used in the determination of the weighting parameters. 44

5.10 Energy resolution and relative difference of reconstructed and deposited energy found when applying the given parametrization of the weighting parameters for jets at a jet angle of $\theta = 17°$ and energies at calibration matrix points. 45

5.11 Energy resolution and relative difference of reconstructed and deposited energy found when applying the given parametrization of the weighting parameters for jets with a jet angle of $\theta = 110°$ and energies at calibration matrix points. 46

5.12 Relative difference of reconstructed and deposited energy in the various calorimeter regions. The data used are preselected jets with a primary electromagnetic fraction larger than 60 %. The $\pm$ 1% and $\pm$ 2% lines are indicated. 48

5.13 Relative difference of reconstructed and deposited energy found in the various calorimeter regions. The data used are preselected jets with a primary electromagnetic fraction larger than 80 %. The $\pm$ 1% and $\pm$ 2% lines are indicated. 49

5.14 Energy resolution found in the various calorimeter regions. The data used (full points) are preselected jets with an primary electromagnetic fraction larger than 60%. The open circles show the energy resolution achieved for all jets The goal (full line) and the energy resolution achieved with the linear calibration ansatz (dotted line) are indicated. . 50

5.15 Energy resolution found in the various calorimeter regions. The data used (full points) are preselected jets with an primary electromagnetic fraction larger than 80 %. The open circles show the energy resolution achieved for preselected jets with an primary electromagnetic fraction larger than 60 %. The goal (full line) and the energy resolution achieved with the linear calibration ansatz (dotted line) are indicated. 51

6.1 Correlation of the total energy deposited in the electromagnetic calorimeter by electrons, positrons and photons (this includes parts of the electromagnetic fraction of hadronic showers starting in the EMC) and the corresponding estimate for the various jet energies in CB2 direction. . . 55

6.2 The full points show the energy resolution obtained using the estimation of the electromagnetic fraction of a jet: $f_{em} = E^{MC}_{estim.}/E^{MC}_{dep.}$; i.e. using MC information in analogy to [Greiff90]. The open circles show the energy resolution obtained with the weighting ansatz without estimation of the electromagnetic fraction of the jets. The full and the dotted line indicate the goal resolution and the energy resolution obtained with a linear calibration ansatz respectively. 56

6.3 The full points show the energy resolution obtained using the estimation of the electromagnetic fraction of a jet: $f_{em} = E^{MC}_{estim.}/E_{rec.}$; i.e: Without using any MC information. E_{rec} is the energy reconstructed with the given parametrization of the weighting parameters for each individual jet. The open circles show the energy resolution obtained with the weighting ansatz without estimation of the electromagnetic fraction of the jets. The full and the dotted line indicate goal resolution and the energy resolution obtained with a linear calibration ansatz respectively. 57

6.4 The full points show the energy resolution obtained using the estimation of the electromagnetic fraction of a jet: $f_{em} = E^{em}_{estim.}/E^{MC,smeered}_{dep}$; i.e.: Using MC information, but applying a gaußian smeering to the MC energy using the experimental resolution found for each individual jet energy when applying the parametrisation of the weighting parameters given previously. The open circles show the energy resolution obtained with the weighting ansatz without estimation of the electromagnetic fraction of the jets. The full and dotted line indicate the goal resolution and the energy resolution obtained with a linear calibration ansatz respectively. 58

List of Tables

1.1 The most propable energy, found by fitting a gaußian function to the data reconstructed on the ideal electromagnetic scale, $E_0^{mop.,\mathrm{gau}\beta}$ and the corresponding energy resolution $\sigma_{\mathrm{gau}\beta}$ is shown together with the design energy resolution for a couple of jet energies and directions. At this level, we observe large systematic shifts of the measured energy with respect to the jet energy. The energy resolution is far from the design value. . 3

2.1 Jet directions used in the calibration of the hadronic response of the H1–LAr–calorimeter. 4

3.1 Statistical and constant contribution to the energy resolution as found by fitting the energy parametrization of the energy resolution to the data. 7

4.1 Summary on the preselection of isolated electromagnetic showers using one estimator only for the example of the EAK0 estimator for an electron identification efficiency of 95%. We show for the available jet data the mean fraction of the electromagnetic content of the jets in EMC, that has been identified ($< f_{tag} >$), the mean fraction of the energy of the generated hadrons, that was misinterpreted ($< f_{fake} >$), the number of events used for the study (N_{total}), the number of events, for which more than 85% of the electromagnetic content deposited in EMC has been correctly identified ($N_{t,85\%}$), and the number of events for which more than 15% of the primary hadronic content of the jet has been faked ($N_{f,15\%}$). It is common to all one–estimator–approaches, that $< f_{tag} >$ is high, but also $< f_{fake} >$ is up to 15%, which is too large for the purpose of hadronic calibration. 16

4.2 Ratio of the energy deposited to the energy reconstructed on the electromagnetic scale for 20 GeV electrons in the electromagnetic calorimeter parts for various noise cuts. 20

5.1 Energy parametrization of the weighting parameters for jets for the various regions of the calorimeter. 33

5.2 Contributions to the energy resolution of the H1–LAr–Calorimeter for the various jet directions. 38

Bibliography

[Greiff90] H. Greiff, Untersuchung zur kalorimetrischen Messung von Jeteigenschaften in hochenergetischen Elektron–Proton Speicherring–Experimenten, MPI–PAE/Exp.El 229 (Juli 1990)

[Dishaw79] J.P.Dishaw, Thesis, SLAC 216 (1979)

[Wellis90] J.P.Wellisch, Untersuchung von Wichtungsmethoden zur Optimierung der Energieauflösung von Hadronen in einem Flüßig–Argon Blei/Eisen Kalorimeter, diploma thesis (October 1990)

[Sirois93] The H1 Calorimeter Group (B. Andrieu, et al.), publication in preparation.

[Gayler91] J. Gayler92 et al. Determination of the Electromagnetic scale for the IF calorimeter, H1–04/91–171.

[Kube94] J. P. Kubenka, Ph.D thesis in preparation

[Wellis91] L. Goerlich, H. P. Wellisch, documentation of the LAr clustering, H1–12/91–204.

[Fabian89] C. W. Fabjan, R. Wigmans, Energy measurement of elementary particles, Rep. Prog. Phys. 52 (April 1989) 1519

[Hadr93] Results from pion calibration runs for the H1 liquid argon calorimeter and comparisons with simulations, The H1 Calorimeter Group (B. Andrieu, et al.), DESY–93–047, (Apr 1993)